MASSACHUSETTS INSTITUTE OF TECHNOLOGY

THE ENERGY LABORATORY

ADVANCED WET-DRY COOLING TOWER CONCEPT
CROSS-FLOW TESTS

by
Troxell Snyder
Jeffrey Bentley
Martin Giebler
Leon R. Glicksman
Warren M. Rohsenow

Energy Laboratory Report No. MIT-EL-77-002 January 1977
Heat Transfer Laboratory Report No. 83307-99 Volume II

TABLE OF CONTENTS

VOLUME II

LIST OF TABLES - VOLUME II

LIST OF FIGURES

VOLUME II

NOMENCLATURE

c	specific heat
D	Diameter
e	rib height
e^+	roughness function
f	friction factor
h	enthalpy
He^+	heat transfer function
ΔH	energy change
K	thermal conductivity
L	length
m	defined by Eq. C-2
$\dot{m}$	mass flowrate
Nu	Nesselt Number
Q	heat flow
r	radius
Re	Reynolds number
Re^+	roughness Reynolds number
St	Stanton number
T	Temperature
t	thickness
$\bar{V}$	Average velocity
$V(r)$	velocity as a function of radius

w	specific humidity
α	flow attack angle
Δ	change
	centerline
η	defined by Eq. C-1
ρ	density

Subscripts

a	air
evap	evaporative
h	hydraulic
ℓ	liquid
o	outside
v	vapor
wv	water vapor

Chapter I: Introduction to Volume II

This volume is the second part of the final project report on the advanced wet-dry cooling tower concept. This was necessary due to time, size and subject considerations. References, table and figure numbers, and appendices used in this volume are unique and are listed in their usual positions. Part I is referred to as Reference [3] throughout while references to particular chapters and sections are taken to be local to this Part.

To help continuity a short discussion of this project history follows. For more information please refer to Volume I of this report.

1.1 Project History

Both the counterflow and crossflow wet/dry cooling towers developed at M.I.T. work in the same manner, the intent of the design is to minimize the air-water evaporative surface area. This is accomplished by confining the water to small channels as shown in Figure 1. Because the plate is constructed of a conductive material, the dry surface in between the channels is heated- resulting in dry heat transfer from the plate to the air. With the plates inclined at a small angle from vertical the water remains in the grooves while flowing downward under the influence of gravity. The packing section is made up of many of these plates (in the opposite direction of the water) while in crossflow the air flows perpendicular to the water (horizontal).

Development of the counterflow packing section was pursued on both an analytical and experimental basis. Using heat and mass transfer correlations, a computer model of the proposed packing section was developed [2]. At the same time an experimental packing section was built and tested in the laboratory [1]. Based on extensive water flow tests, the counterflow plates were constructed as shown in Figure 2.

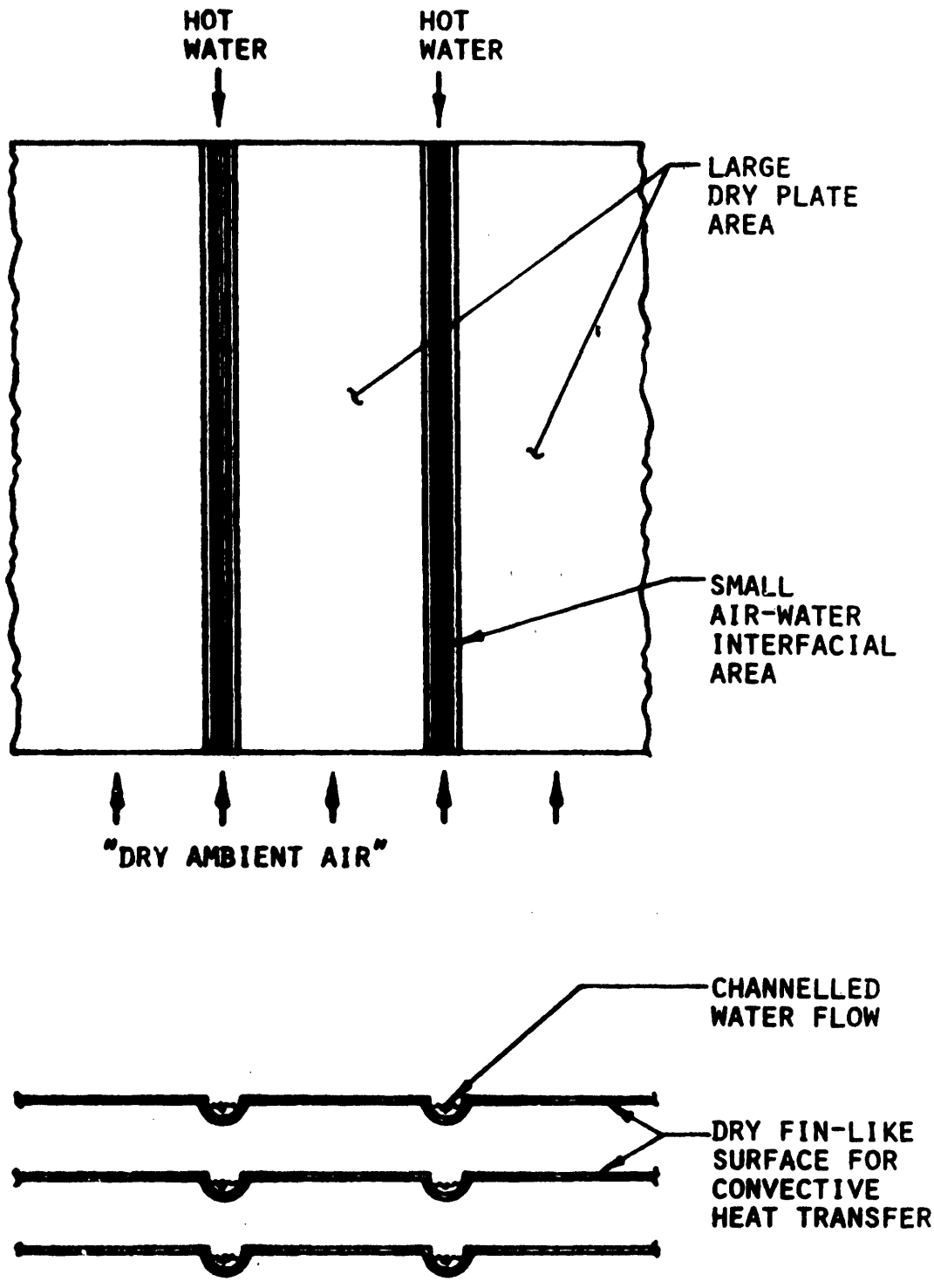

FIGURE 1. CONCEPTUAL DESIGN OF THE NEW WET-DRY SURFACE

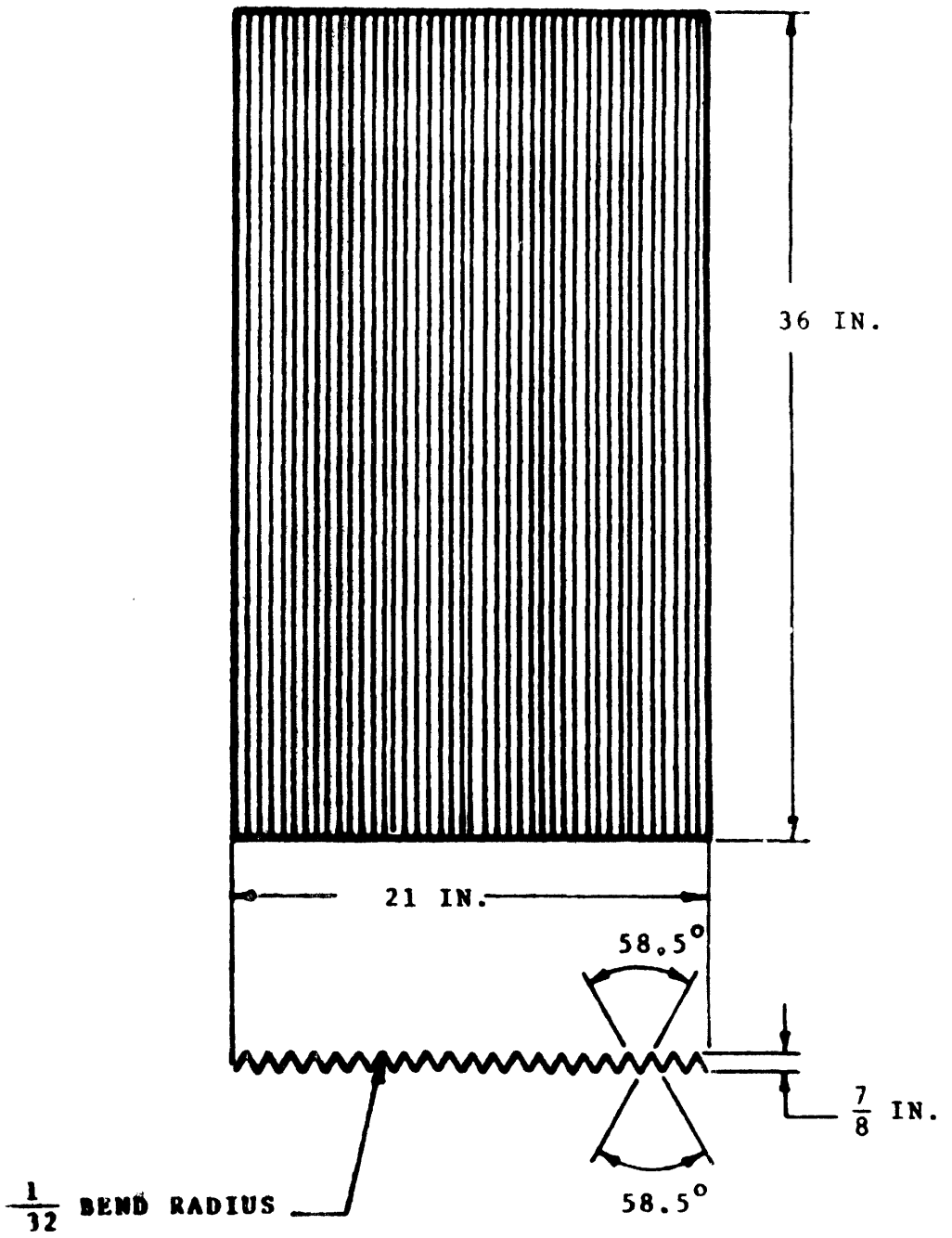

FIGURE 2 V-TROUGH PACKING PLATE

The material used was .018" (.046 cm) galvanized steel. Fourteen of these V-trough plates were used to form the packing section. The angle of inclination was 10 degrees. Figure 3 shows the entire counterflow test apparatus. For a complete description of the counterflow test apparatus construction and operation the reader is referred to reference [1].

As shown in Figure 3, hot water enters the feeder tanks which supply the distribution pipes at the top of the packing section. Holes drilled in the distribution pipes line up with each V-trough of the packing section such that a jet of hot water impinges at the base of each trough near the top of the packing section. The water is cooled while flowing down the plates. Collecting channels and a drain box then remove the water to reservoirs. Air flow is in the opposite direction (up the plate) as described earlier.

To evaluate the tower performance, the counterflow tower was instrumented to measure flowrate, temperature and air humidity. Experimental data were obtained for a variety of conditions and compared to the predictions of the counterflow computer model [2], [3]. The tests showed that the V-trough packing section in the counterflow arrangement reduced the evaporative heat transfer to about 40% as compared to 85% for the totally wet tower. In addition the predictions of the computer program were reasonably accurate. The counterflow tests verified the accuracy of the computer program in predicting the behavior of the counterflow wet/dry surface. Because of this verification, the computer program could be used as a design tool for a full size wet/dry counterflow cooling tower.

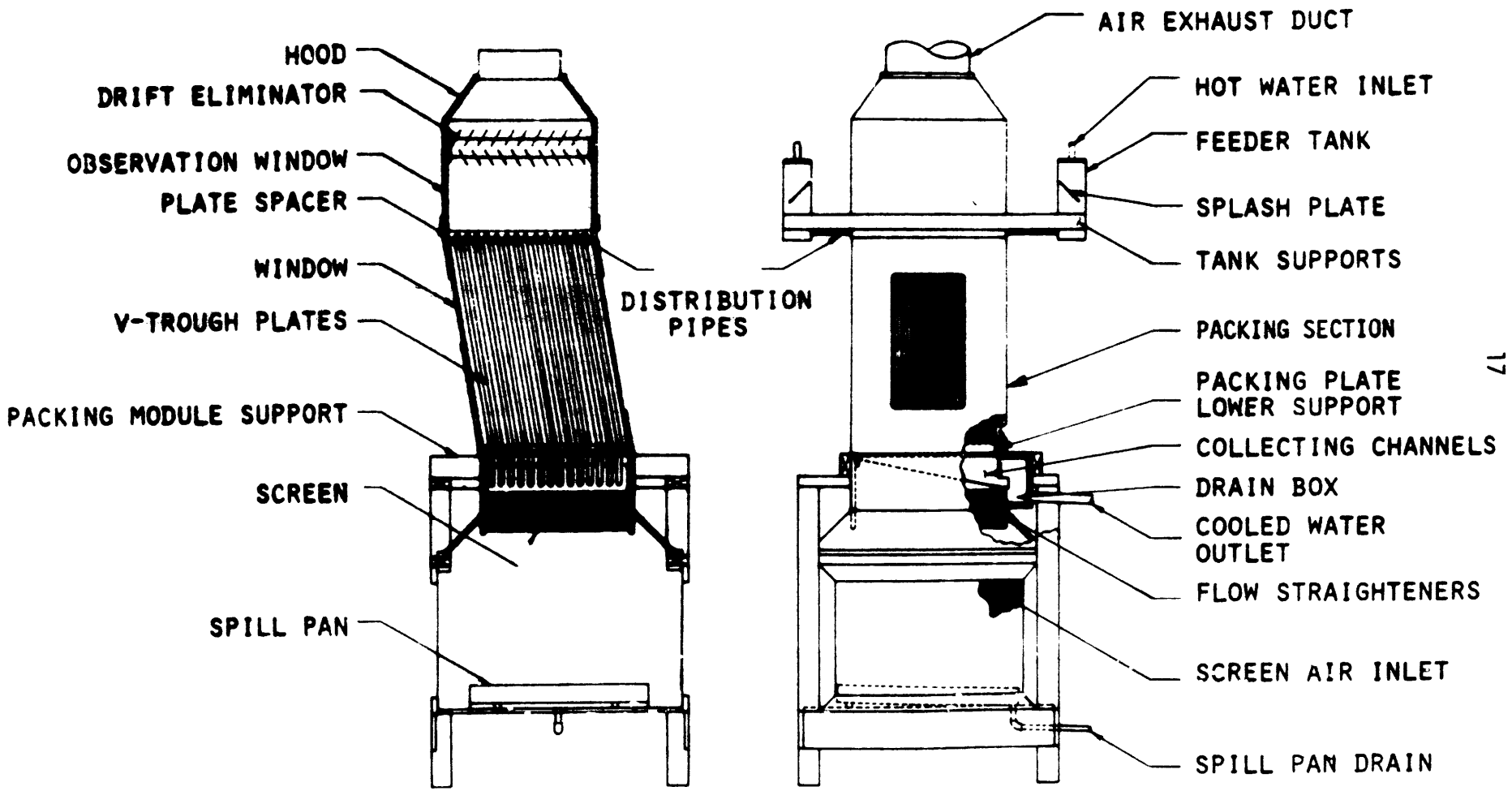

FIGURE 3. HEAT TRANSFER TEST APPARATUS ASSEMBLY

Experience with the experimental counterflow tower revealed several deficiencies inherent to the counterflow configuration. The most serious problem arose from the fact that the air and water stream had to cross at the top and bottom of the packing section. The most obvious difficulty with this arrangement was header design. The water distribution and collection systems had to be designed so that airflow through the packing section was possible. This fact complicated the counterflow design. As described earlier, the distribution system was comprised of feeder tanks and a distribution pipe for each plate.

In order to compete with the low cost of a wet cooling tower, any feasible design of the wet/dry cooling tower must be simple. This rules out elaborate header designs. Even the distribution system used in the counterflow experimental apparatus was too complex, requiring a large amount of machining and materials. But the complexity (and cost) of header design is inversely related to the amount of a free water surface exposed to the air during distribution and collection. Any air-water surface area which will lead to evaporation is a cooling tower. The simplest, cheapest design for water distribution would be a series of showerheads over the packing section. An even distribution of drops would fall onto the plates and eventually be channeled to the bottom of each groove. However, while each drop falls through the air, very significant evaporation can occur. More expensive distribution systems could be devised in an effort to shield water from air until the point might be reached where each trough would have its own feeder line. This type of design approaches the complexity of a dry cooling tower.

Evaporation and heat transfer in the collection system of the experimental counterflow apparatus had the effect of preheating the intake air before it reached the packing section. This made it impossible for the packing section to be tested at low inlet air temperatures. Higher inlet air temperatures tend to reduce dry heat transfer while evaporation remains constant. This is counterproductive to the objective of reducing evaporation. The problems noted above made the counterflow configuration undesirable from an experimental standpoint. The need to design a more complicated water distribution system made it undesirable from a commercial standpoint.

1.2 Scope of This Work

To eliminate the problems mentioned above development of a cross-flow packing section was proposed. The water would travel the same path as before but the air stream would enter and exit from the sides of the packing section. This would eliminate the header and air preheating problems. Also, it would be much easier to protect those areas where the water must fall freely through the air (distribution and collection areas) from the main air stream. Now a simple spray type distribution might be feasible. Additional benefits were anticipated from the switch to crossflow that would make it commercially a more practical design. Besides the lack of complicated headers, the crossflow design is simpler to implement on a large scale and is already widely used on wet towers. For a more comprehensive discussion of the commercial feasibility of a crossflow wet-dry cooling tower the reader is referred to [3].

An even more important advantage that was foreseen was the anticipated increase in the heat transfer coefficient in the crossflow configuration. The result would be a more compact cooling tower for a given heat rejection load. The reason for the increase in the heat transfer coefficient can be seen by referring to the drawing of the V-trough plate, Figure 2. In counterflow, the air travels up the grooves and a boundary layer grows undisturbed along the entire plate. Thus, the heat transfer coefficient will be better in the lower regions of the plate where the boundary layer is not fully developed. However, in crossflow, the profile of the channel is perpendicular to the air flow. Each channel serves to break up the boundary layer and increase the local heat transfer coefficient.

This feature is not without its drawbacks however. Any increase in the heat transfer coefficient will lead to a comparable increase in the mass transfer coefficient. This means that, although the crossflow design should lead to a more efficient transfer of heat, the percentage of heat transfer by evaporation could be expected to be similar to the counterflow. Other problems could be expected to occur if the trough profile were made too large. In this event, recirculation of air over the water surface could increase evaporation. Also, a larger profile could lead to a great increase in the fan power necessary to move the air by creating a large pressure drop across the packing section.

Because of these last two considerations, it was decided that a new packing surface would be necessary to fully realize the advantages

of crossflow while minimizing the disadvantages. Development of a new surface would allow design of a packing plate which would present a smaller profile to the airflow. Also, different plate materials and manufacturing techniques could be investigated.

As with the counterflow design, development of the crossflow packing section was pursued on both an analytical and an experimental basis. The body of this thesis will deal with the design, construction and testing of the experimental crossflow apparatus. The crossflow computer model is presented and described in Volume I of this report.

Chapter 2 discusses the conversion of the counterflow apparatus to crossflow. The design and manufacture of the crossflow plates is detailed in Chapter 3. Instrumentation is taken up in Chapter 4. Chapter 5 presents the experimental data obtained from the crossflow packing section and compares it with the computer model predictions. Conclusions and suggestions for further work can be found in Chapter 6.

CHAPTER 2

CROSSFLOW EXPERIMENTAL APPARATUS

2.1 Apparatus Requirements

This chapter presents the details of the design and construction of the crossflow model tower experimental apparatus. The main goal of the project was to test the heat and mass transfer performance of the wet-dry packing section in the crossflow configuration. The apparatus necessary to perform these tests would, in many ways, resemble a conventional wet tower.

To simulate the cooling demands of an actual tower, hot water was supplied to the water inlet of the model tower. As with conventional towers, airflow was of the induced draft type. It was desired to maintain the experimental conditions for the model tower similar to those found in actual wet cooling towers. Thus, the range of air and water flowrates, inlet temperatures and temperature changes were to be determined by actual cooling tower conditions. To aid future plans for the commercial production of a wet-dry tower of the type discussed here, a good deal of attention was given to the commercial feasibility of the design.

The counterflow experimental model was in good working order in the laboratory. Therefore, the experimental program was planned so that crossflow data could first be taken on the V-trough plates in place in the packing section at the time. So the first step was to convert the

counterflow experimental apparatus to crossflow. Then, data could be taken on the V-trough plates while the crossflow plates were being designed and manufactured. Since the crossflow model tower was to be tested first with the V-groove plates from the counterflow model tower, the most practical crossflow design allowed an almost complete retrofit of the counterflow packing section described in the Introduction.

2.2 Airflow Design

In a typical wet cooling tower, air speed averages 600 fpm It was necessary to produce this air speed using the fan from the counterflow apparatus. Testing of the counterflow apparatus had determined that the fan was capable of delivering 1400 cfm (427 m/m) at a pressure drop of .5 in of water (1.23×10^{-3} atm.). Analysis of the system showed that most of this pressure drop in the counterflow tower occurred when accelerating the air to the velocity in the duct just ahead of the fan (about 30 fps (9 m/sec)). It was anticipated that the magnitude of the frictional pressure drop and the final duct velocity would be similar in the crossflow tower. Hence, for use in the crossflow model tower the fan could be expected to deliver approximately the same volume flowrate as it had in the counterflow apparatus. To produce a packing section air velocity of 600 fpm (183 m/min) required an air flow area of 2-1/3 ft^2 (.217 m^2).

The required airflow area was most easily realized by cutting similar air inlet and outlet flow passages in the sides of the packing section. To use almost the full height of the V-trough plates, the

duct height was set at 27" (.686 m). A duct width of 12" (.305 m) produced the suitable air flow area of 2-1/3 ft^2 (.217 m^2). With a plate spacing of 1.5 in (3.81 cm) this duct width allowed for 7 test plates.

2.3 Water Flow Design

The water channeling ability of the V-trough plates was studied extensively in reference [1]. As a result of these studies the plate inclination was set at 10° from the vertical. This inclination allowed effective water channeling by the V-troughs while maintaining a fast water velocity in the trough. Since this plate inclination had performed well in the year of testing the counterflow model tower, there was no reason to change it for the crossflow tower. It remained to be seen if this inclination would allow the crossflow plates to perform properly.

With the airside velocity and flowrate set, a water flowrate range was chosen. Typical water mass flowrates in conventional cooling towers are about half that of the air mass flowrate. Thus, the design water flowrate was chosen to be 55 lbm/min (25 Kg/min). The water pump and metering equipment from the counterflow model were capable of delivering up to 170 lbm/min (77 Kg/min) to the water inlet, allowing considerable water flowrate margin on either side of the design flowrate.

2.4 Apparatus Construction

The major task involved in construction of the crossflow model

tower was reworking the packing section to accommodate the air and water distribution systems. The conversion of the V-groove counterflow packing section will be discussed here. Installation of the new plates into the packing section box is discussed in Section 3.4.

The packing section box houses the plates, aligning them in the proper fashion and holding them in place. It also seals the packing section from the laboratory environment and channels the airflow. Because the V-groove plates were already installed in a packing section box with the proper plate angle and spacing, conversion to crossflow was much simpler. Almost half of each side of the box was cut away for the air inlet and outlet with dimensions previously calculated (see Figure 4). The rear of the packing section box was not used to house plates, but did serve as a structural support for the cut away portions of the box.

An air inlet duct was constructed from 3/4" (1.91 cm) plywood as shown in Figure 5. 6-1/4 inches (15.88 cm) by 1/4 inches (.64 cm) diameter plastic drinking straws were used as flow straighteners in the inlet duct. The straighteners eliminate any eddys in the inlet air and provide a uniform air velocity entering the packing section.

The design of the air outlet header is shown in Figure 6. The header is the transition piece from the 27-1/2" (69.85 cm) by 12-1/4" (31.12 cm) parallelogram shape of the packing section air outlet to the 14" (35.56 cm) diameter circular air duct leading to the fan. The transition needed to be gradual in order to insure uniform air velocity along the top and bottom of the plates in the packing section.

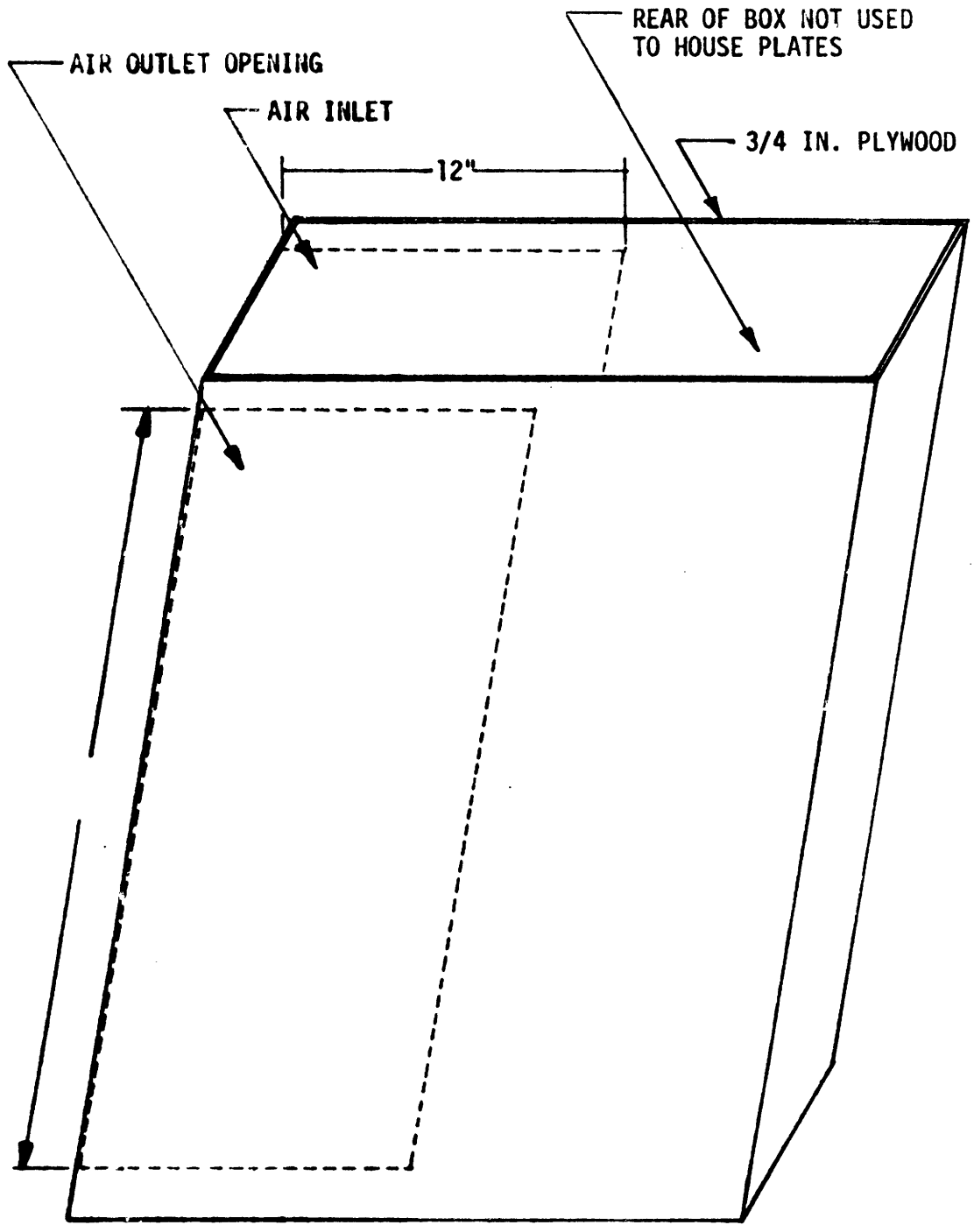

FIGURE 4. MODIFICATIONS TO PACKING SECTION FOR CROSSFLOW

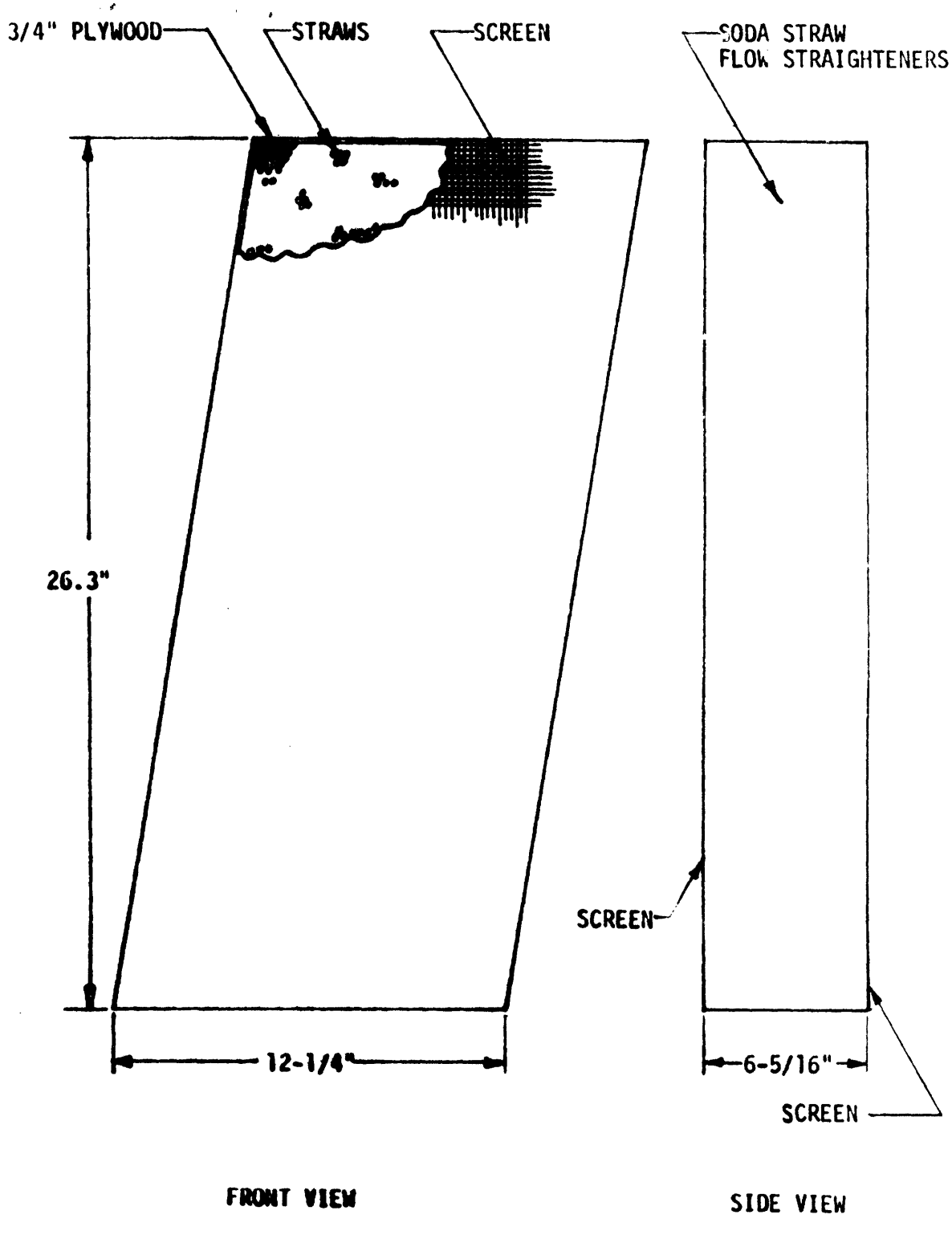

FIGURE 5. AIR INLET HEADER

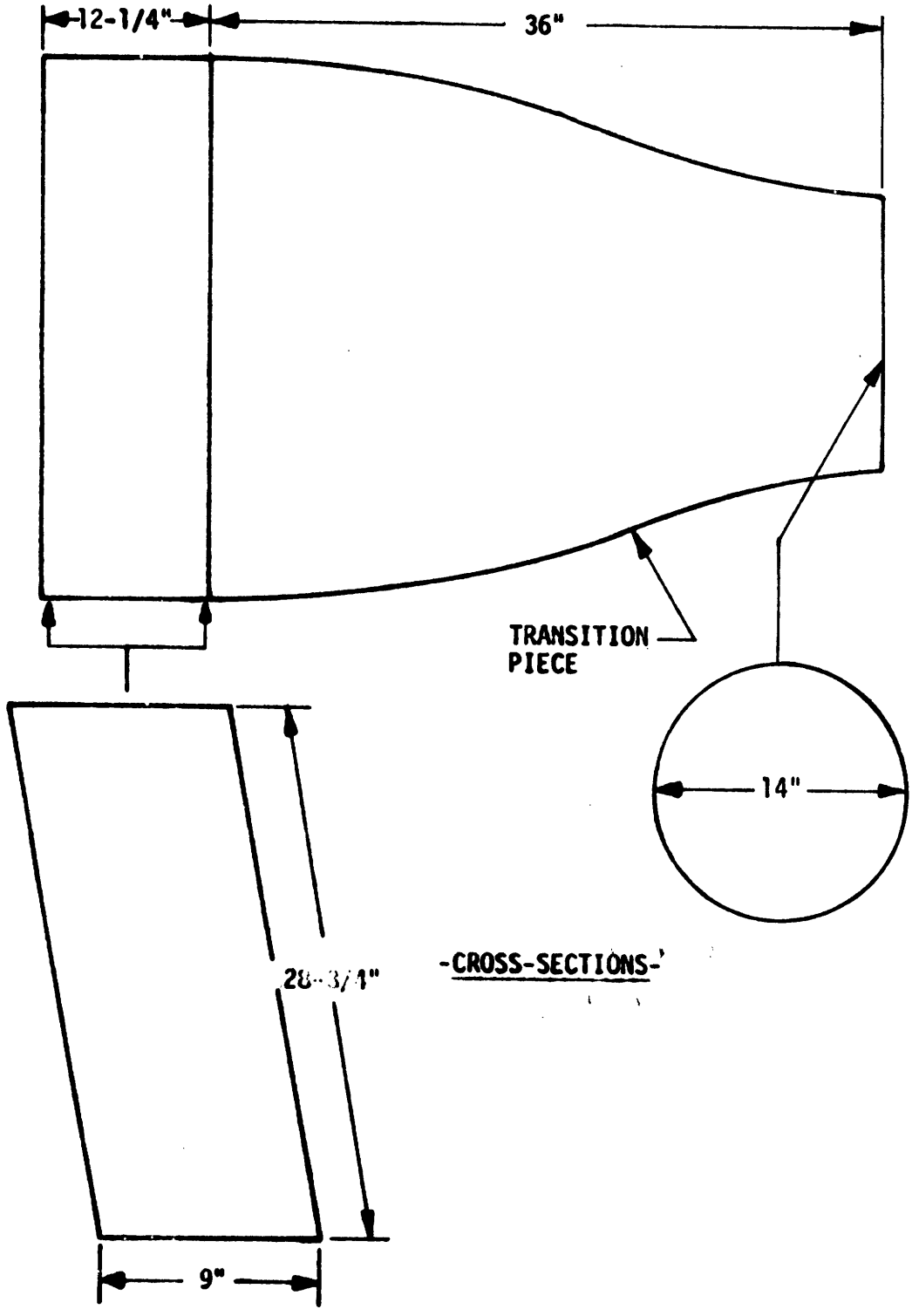

FIGURE 6. OUTLET HEADER

Fabrication of the outlet header by a sheetmetal shop was rejected as being too expensive. Also, smooth curves of the type needed here are difficult to fabricate from sheetmetal. Instead, the transition duct was fabricated by hand. Welding rod was used to form a skeleton in the desired shape. Window screen was then used as a skin. To make the duct airtight, alternate layers of thick latex paint and duct tape were applied over the screen.

Testing of the counterflow model tower had been complicated by the methods necessary to determine the air mass flowrate. Because no place could be found to measure an average air velocity, a scan of 9 points was made for each run. This scanning technique was tedious to perform and susceptible to errors. The design of the crossflow tower included a long run (12 L/D's) of straight ducting between the outlet header and the inlet to the fan. An average air velocity measurement could then be made at some point in the duct downstream of the disturbances created by the packing section and upstream of any distrubances the fan might create. Air flow instrumentation is discussed in Chapter 4.

Because the waterflow equipment used in the counterflow tower had proven adequate, the only major design necessary for the crossflow conversion was for water distribution and collection in the packing section. Before describing the distribution and collection schemes employed, the other flow equipment shown in Figure 7 will be described.

Outlet water from the packing section collection system drains into an exit trough (1). Three 1-1/4 in. (3.18 cm) copper drain pipes

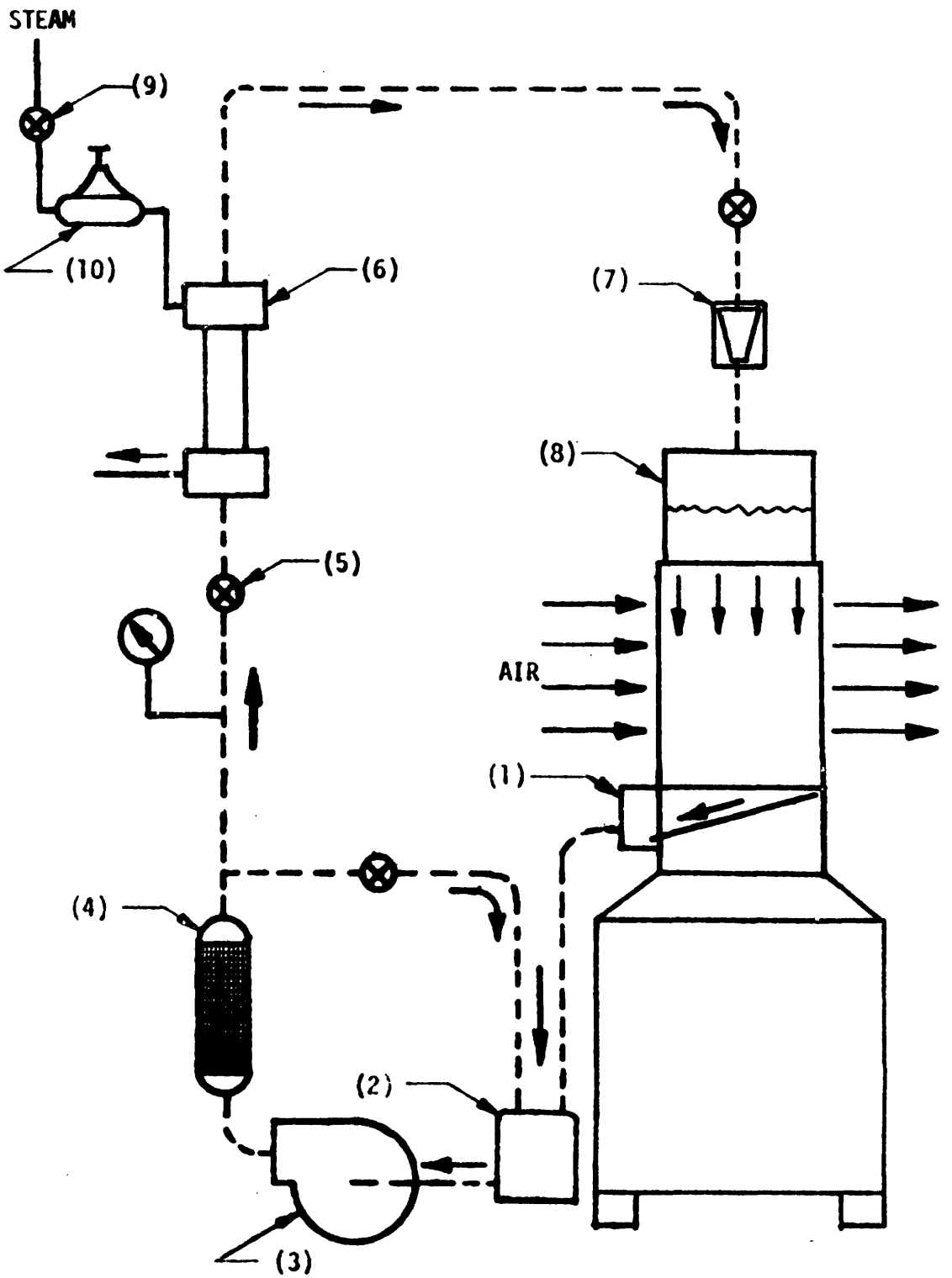

FIGURE 7. PLUMBING SCHEMATIC OF EXPERIMENTAL APPARATUS

recycle the water into two 20 gallon (78 ℓ) galvanized reservoirs (2). These reservoirs supply the pump (3). From the reservoirs, the water is pumped through a filter (4), metering valve (5) and the steam-water heat exchanger (6) before entering the rotometer. Heated water coming out of the rotometer travels overhead to the water distribution tank (8) atop the packing section. Temperature of the water coming out of the heat exchanger is regulated by controlling the steam supply to the exchanger with the steam metering valve (9) and steam pressure regulator (10).

Water distribution for the counterflow tower was complicated by the need for the air and water streams to cross at the top and bottom of the packing section. In crossflow the airflow is perpendicular to the water flow and this problem is eliminated. Thus, the simplest design for distributing the water was simply a plexiglas box with holes drilled at proper spacings in the bottom to provide water streams to each trough in the packing section. The water flowrate through the holes is governed by the head of water in the tank. The head is equal throughout the box insuring equal flow through each hole. In addition, construction from plexiglas allowed visual inspection of the inlet water head. Thick plexiglas (3/8 in. (.95 cm.)) was used to minimize heat loss from the tank.

As with the distribution system, design of a water collector for the crossflow tower was simplified. Water falling off the bottom of the plates is caught by a plexiglas collection pan. The collection

pan slopes toward the collection trough described earlier, dumping water into the trough for return to the reservoirs.

The assembled crossflow model tower is shown in Figure 8. Because the V-groove plates lacked sufficient rigidity to bending along the grooves, 3 spacers of the type shown in Figure 9 were inserted at the top and bottom to hold the plates rigid. These spaces also served to limit airflow at the top and bottom of the plates. Rubber flaps attached to these bottom baffles extended down to the collection pan. These flaps float on the water surface in the collection pan, allowing water to pass underneath while blocking air flow over the water surface. These flaps prevented airflow over the free water surface area in the collection pan, helping to eliminate the evaporation contribution from the collection system.

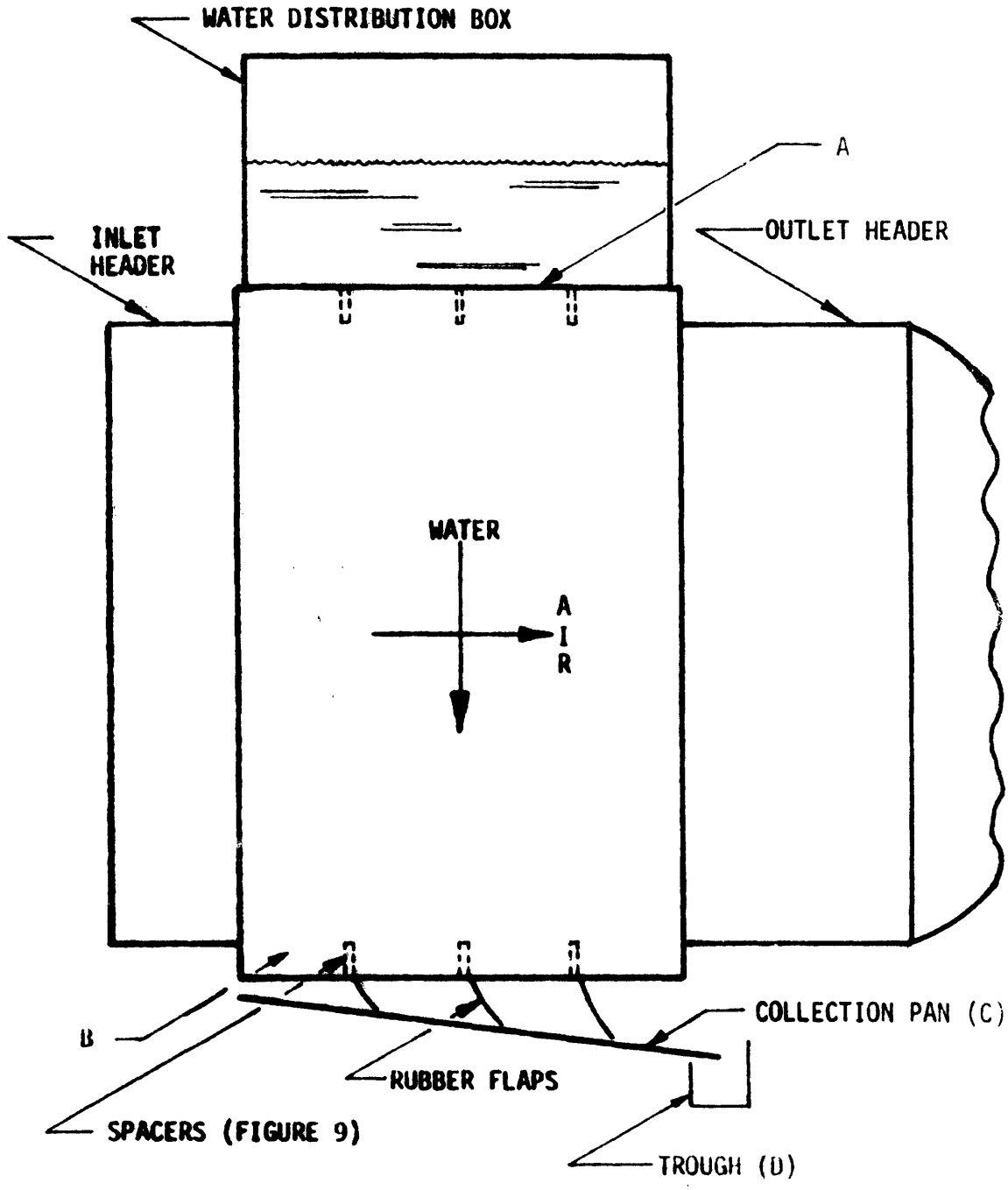

FIGURE 8. ASSEMBLED EXPERIMENTAL APPARATUS

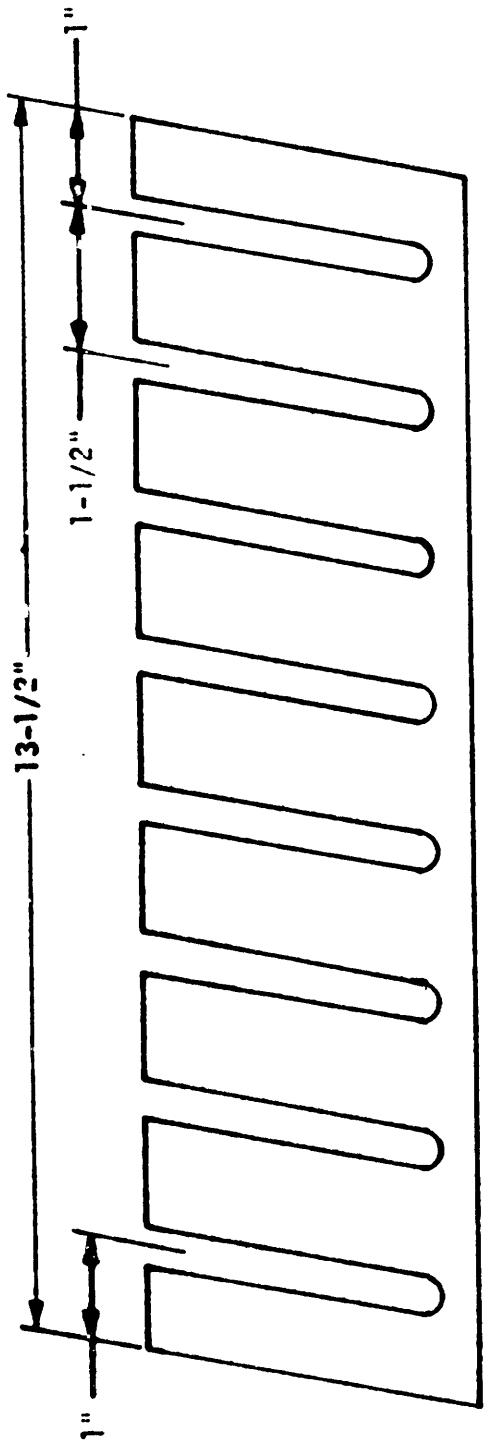

FIGURE 9. PACKING PLATE SPACER

CHAPTER 3

CROSSFLOW PACKING PLATES

This section discusses the design and manufacture of new plates for the crossflow packing section. The V-groove design of the counterflow plates was not considered optimal for crossflow because of the large profile presented to the new air flow direction. To reduce the air pressure drop across the packing section and to prevent air recirculation over the water surface it was necessary to design a new plate with a smaller trough depth. At the same time, the redesign of the plates made it possible to explore more efficient plate configurations and different methods of producing the plates. The design of the plates and their production is taken up in the following sections.

3.1 Plate Design

The foremost consideration in designing the crossflow plates was to create a packing section that would be a realistic prototype of a commercial packing section. The intent was to design a plate that performs properly and can make maximum use of materials while keeping manufacturing cost at a minimum. In a manufacturing operation where thousands of plates might be produced, a pressing or rolling operation would undoubtably be the cheapest production method to form the shallow grooves needed for the crossflow plates. For this reason the decision was made to press the plates for the crossflow experimental model tower.

Because of its suitability for pressing, the plate material chosen was .025 in. (.064 cm.) thick half hard aluminum. The increased thermal conductivity of aluminum allowed the spacing between water troughs to be increased over the 1 in. (2.54 cm.) spacing of the steel V-groove plates while maintaining a similar fin efficiency. Appendix C presents the details of the fin efficiency calculations. The plate is modeled as a fin with base temperature equal to the water temperature in the trough. For a fin efficiency of 85% the trough spacing is calculated in Appendix C to be 3 in. (7.62 cm.). The width and height of the plate, as shown in Figure 10, was chosen to allow the new plates to fit in place of the V-groove plates with little alteration of the packing section box. As shown in Figure 10 the chosen plate width and trough spacing gives 7 troughs per plate.

With the overall plate dimensions and number of troughs set, the trough dimensions were considered next. The three considerations in determining the trough dimensions were: percent total wet area desired, minimization of the profile presented to the air crossflow and ability to handle the necessary water flowrate. In light of the last two considerations noted above, it was decided to construct a trough with no more than three times the water flowrate area (trough cross-sectional area) as used in the counterflow V-grooves. Photographic studies of the V-groove plates had determined that the water surface area for the 60° troughs was 3/16 in. (.473 cm.). This dimension was found to be substantially independent of water flowrate (over the

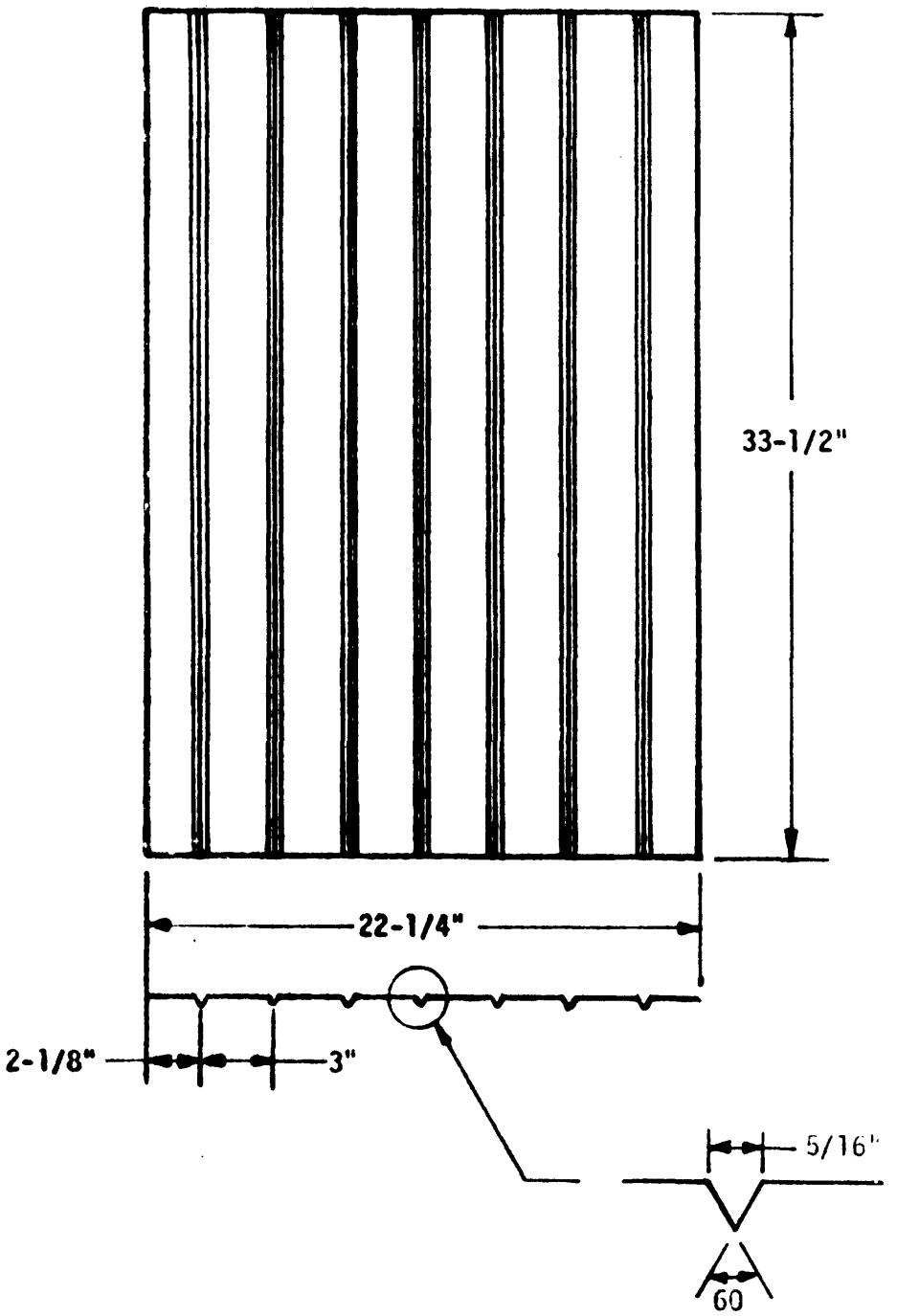

FIGURE 10. PROPOSED CROSSFLOW PACKING PLATE

range normally encountered during counterflow operation). Since the anticipated crossflow water flowrates were in this same range, the trough shape was chosen to be a 60° equilateral triangle, 5/16 in. (.794 cm.) on a side. This design gives a water flowrate area of 3 times the counterflow water flow area, leaving a good margin to prevent water from straying out of the troughs. This trough design depth is less than 1/4 in. (.635 cm.). Since the planned spacing between plates was 1.5 in. (3.81 cm.) this profile is small enough to avoid large air pressure drops. The wet surface area (based of a 5/16 in. (.794 cm.) water surface area for each trough) is 5%, a value similar to the counterflow model tower. This similarity would allow comparison of the test results from the two types of towers.

3.2 Plate Production

With the plate designed, the next step was to design a press to construct the plates. The design was created with an emphasis on maintaining uniform trough spacing. Uneven trough spacing on the V-groove plates had made it necessary to locate and drill each water jet hole in the distribution box individually. Evenly spaced troughs would make locating the proper position of the water jet holes in the distribution box easier and more accurate. This would reduce the chance of a misaligned water jet spraying water out of the channel. To maintain uniform spacing, a type of double press was designed as shown in Figure 11. The operation would begin by pressing the initial groove in the aluminum sheet with the stamping block. Then this first groove

would be moved to the index side and clamped by the index block. The next groove would then be formed by the stamping block. The clamping action of the index block would prevent material from between the two troughs from creeping under the stamping block. In this manner precise spacing of the troughs could be obtained.

Because the aluminum could not be expected to deform to the trough shape without tearing, extra material would have to move in from the undeformed part of the sheet as shown in Figure 11. This problem increases as the pressing block moves down into the groove and the bends at points A and B become sharper. To avoid splitting the aluminum, these two points must be rounded and well lubricated.

Before attempting to construct a press for a full size plate, a small test press was constructed. This allowed, without excessive material waste, the testing of the plate design and press theory just presented. Also, the smaller pressing force could be developed with an arbor press instead of the cumbersome pressing apparatus needed for a full sized sheet.

The 6 in. (15.24 cm) test press was constructed as shown in Figure 11. The male and female presses were milled to the trough dimensions and spacing presented earlier. To avoid material cutting and spliting, a rule of thumb for pressing operations was used; sharp corners must be rounded to at least three times the metal thickness. This was done at the two critical edges of the press discussed earlier.

Using 4 in. (10.16 cm.) aluminum strips, 4 in. long test plates were easily pressed using an arbor press. With the critical points

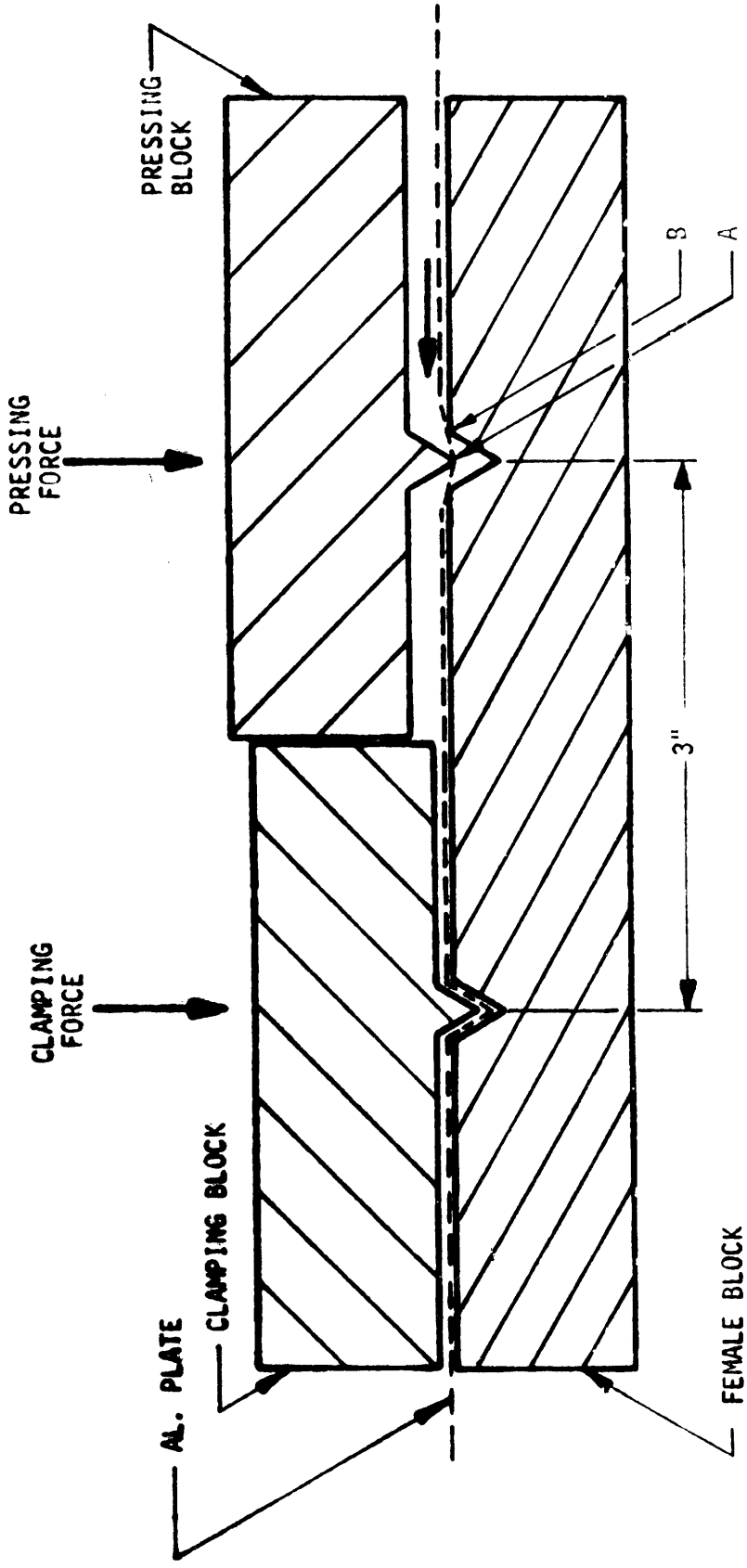

FIGURE 11. PROPOSED PRESS FOR CROSSFLOW PLATE MANUFACTURING

rounded and using petroleum jelly as a lubricant, no cracks developed. Prior to pressing, some aluminum strips were softened by heating with an acetylene torch and then allowed to air cool. This softening resulted in a reduced pressing force necessary to obtain the desired shape. However, any other possible effects of the heat treatment on the metal were unknown. Also, heat treating a large plate uniformly was considered impractical.

The plates pressed in the test press showed less than .010 in. (.025 cm.) variation in trough spacing over 7 troughs, quite adequate for the desired application. The trough shape was not as well defined as expected. The 3 trough corners were not sharp but instead had a radius of about 1/16 in. (.159 cm.). This rounding contributed to a reduction in water flowrate area. To assess their water channeling ability, water tests were conducted on test strips held at a 10° inclination. Tests with flowrates up to 2 times the expected maximum revealed no water straying out of the 4 in. long troughs. On this basis it was concluded that the water channeling ability of the troughs was adequate if care was taken to insure that each jet from the water distribution box sprayed into the center of each trough.

Measurements of the aluminum strips before and after pressing determined that the irreversible (plastic) strain of the material was only 1/64 in. (.040 cm.) per trough. Since this amounted to less than 1/8 in. (.318 cm.) over 7 troughs no corrective measures were necessary. Because the first and last troughs of each test plate appeared to be

of inferior quality it was decided to press the full sized plates with 9 troughs and shear off the end troughs.

Based on the favorable results of the test press, a full sized press was constructed as shown in the same manner. The press length was increased to 36" (.96 m). Guide holes and pins were added to the pressing block to insure that the press would be centered properly over the female block. The indexing press was equipped with 2 hex bolts at either end to apply the clamping force. A 4 in. (10.16 cm.) I-beam was welded to the top of the pressing block. This reduced the deflections at the press ends and allowed a single pressing force to be applied at the center.

According to plastic hinge theory, the necessary pressing force was estimated to be approximately 10 tons (9.07 tons). To develop the force a 20 ton (18.14 tons) hydraulic jack was used. The female press was clamped to a cast iron test bed. A heavy truss consisting of channel and angle iron was constructed over it. The jack was placed between the pressing block and the bottom of the truss to apply the pressing force. To aid the clamping force of the 4 hex bolts, three adjustable struts were placed between the index press and the overhead truss. The center portion of these struts was a turnbuckle. Twisting the turnbuckle applied the clamping force to the index press to prevent the plate underneath from pulling during the pressure operation. Pressing of the plates proceeded just as with the test plates. The critical corners of the press periodically developed burrs due to the sliding

motion of the aluminum. These burrs had to be filed off to prevent them from cutting the aluminum.

Eleven plates were manufactured. Each was sheared to the desired width. To prevent corrosion, each plate was coated with a heavy layer of clear anodization. Stress developed in the pressing operation caused the plates to curl along their width. This problem was corrected by attaching 1/2 in. (1.27 cm.) aluminum angles at the top and bottom of each plate as shown in Figure 12.

3.3 Surface Roughеners

It has been shown [4] that the use of surface roughеners to augment heat transfer can be cost effective. On the plates described here, the protrusion of the troughs into the air stream should serve to break up the boundary layer on the back of the plates. Thus, the backs of the plates should have a naturally high heat transfer coefficient. The front of the plate is essentially a flat plate. To increase the front side coefficient, consideration was given to the use of ribs to augment the heat transfer on the front of the plates. In addition, such roughеners, if placed at an angle from the vertical, could serve to channel any stray water streams or drips back into the troughs.

Reference [4] presents two guidelines for the use of ribbed surface roughеners. First, the optimal angle of attack is 45° from the airflow direction. Second, the ratio of rib spacing to rib height should be about 10 to 1. Using 1/4 in. (.64 cm.) aluminum stock for ribs the spacing was set at 2.5 in. (6.35 cm.).

Figure 12 shows how the rougheners were applied to the plates. The ribs extended only to the edges of the troughs. Thus, any water that might stray between the troughs would be channeled to the next trough. This would help reduce the evaporative water surface area in the event of water straying out of the channels. The angle of the ribs was set so that air flow would be channeled toward the middle of the plate. This feature would help reduce the airflow across the distribution section (top) and collection pan at the bottom. Because the rib height is only 1/6 of the channel width, the effect is slight. The rougheners were applied to the plates using a "super glue" contact cement. The glue bonds quite well unless the plate is flexed or jarred.

The method described here for producing the surface roughness was very laborious and would be unsuitable for commercial production of crossflow plates. One practical method might be to stamp the desired profile at the same time as the grooves. However, there is a limit to the amount of distortion the sheet metal can undergo before it tears. A more feasible method might be to use tabs cut directly from the plate. This idea is shown in Figure 13. Three sides of the desired profile are cut out of the sheet. The tab is then bent up perpendicular to the plate using the uncut side as a hinge. This method would produce only a 2-dimensional roughener. This will not greatly affect its ability to increase the heat transfer from the plate and the cost of implementation would be very low.

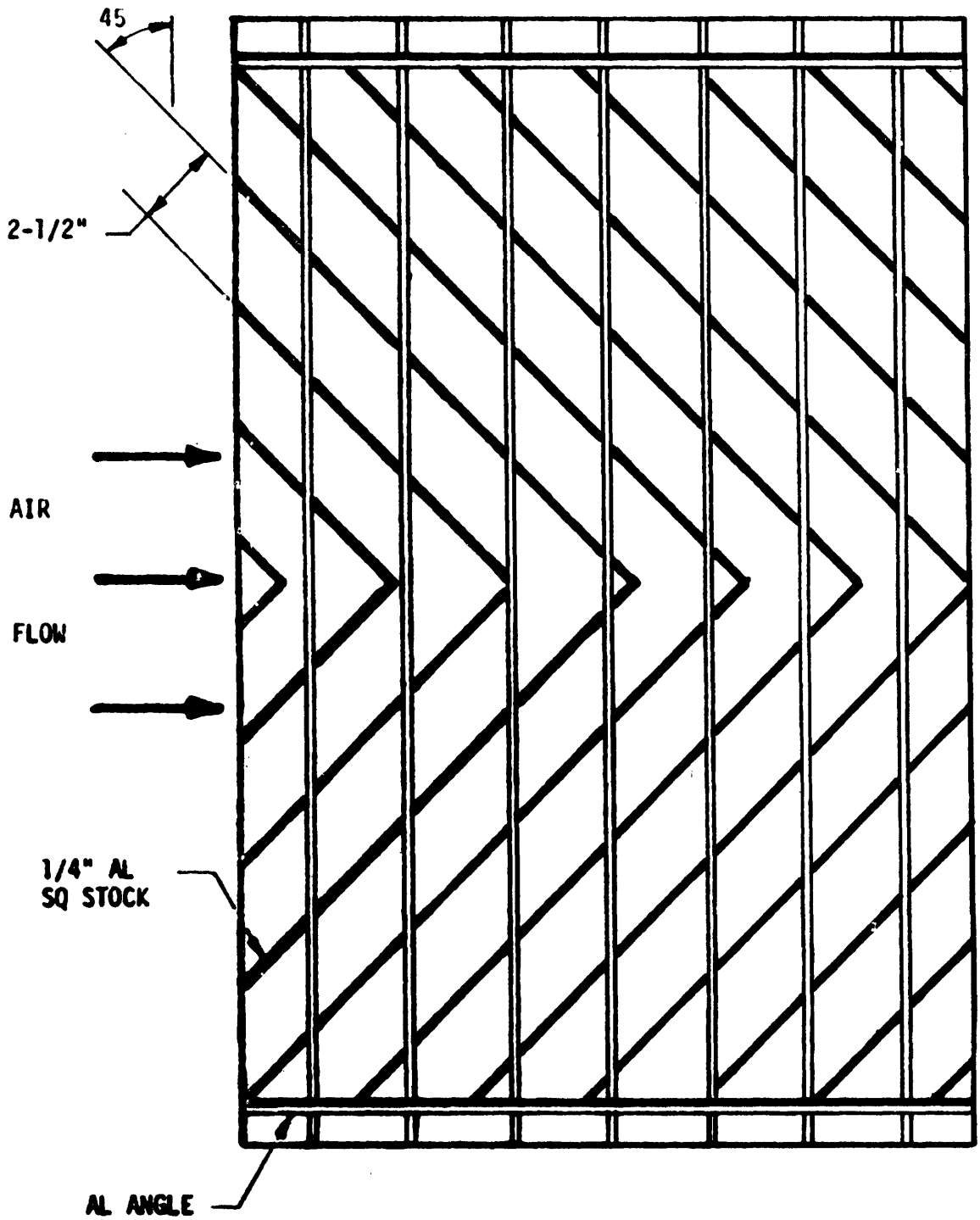

FIGURE 12. CROSSFLOW PLATE WITH ROUGHENERS

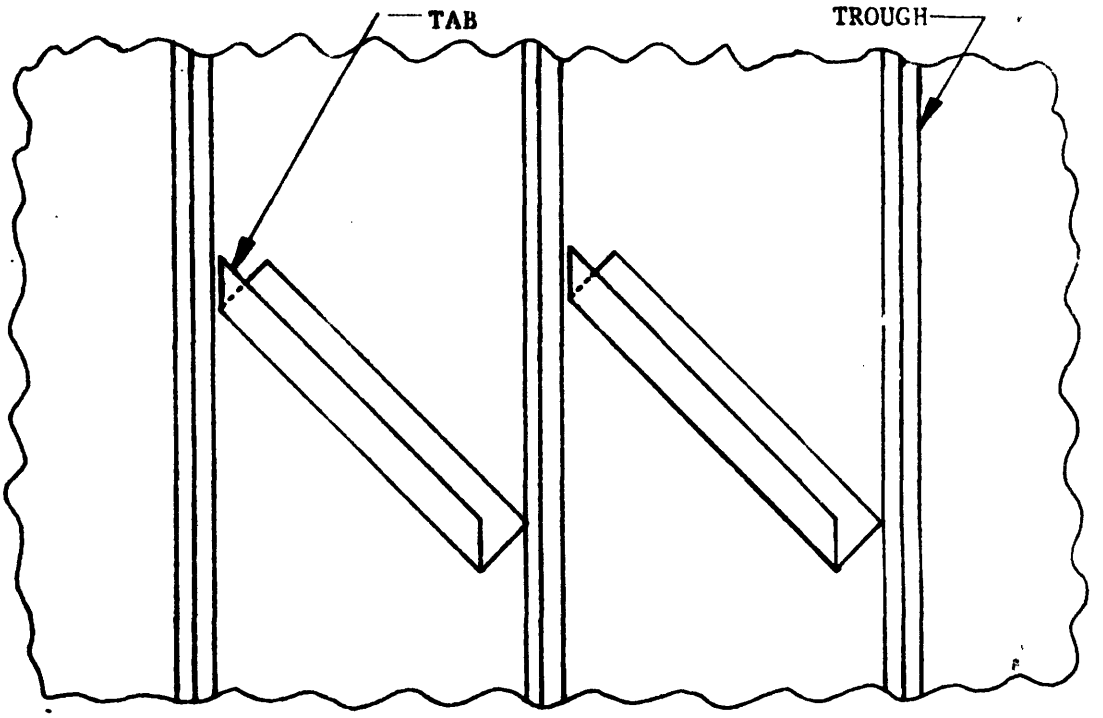

Figure 13. USE OF TABS FOR PLATE SURFACE ROUGHENERS

3.4 Installation in the Experimental Apparatus

The new plates were installed in the packing section in a manner similar to the V-groove plates. Holes drilled in the corners of the plates allowed them to hang on 7/16 in. (1.11 cm.) rods running through the box. The top of each plate fits flush against the bottom to the distribution box. Water jets from holes drilled in the box line up with the troughs at the top of each plate. Correct spacing between plates was insured by fitting wooden spacers over the rods between the plates.

Although only 7 plates were installed to transfer heat, an eighth identical plate was installed as the back of the packing section. This plate serves as a dummy to isolate the packing section

from the rest of the housing box. This plate plays no role in heat exchange and there is no water flow in the troughs. It was installed to insure that the airflow in the last space would be the same as between any two other plates. A smooth back to the packing section would lead to a greater flow in this last space.

To avoid airflow over the water distribution and collection areas of the model tower, plexiglas baffles were inserted between the plates. These were then sealed in place with modeling clay. This precaution was necessary to prevent evaporation in other areas from masking heat and mass transfer results from the test surface. Commercially this same result could be achieved in many different ways. One alternative would be to manufacture plates with baffles as an integral part. Attached to the front of the plate, each baffle would mate with the back of the next plate. This would serve the dual purpose of insuring correct spacing and properly channeling the air. Although the method of baffling used in this experiment would be unfeasible in a commercial operation, the end result could be achieved in a cost effective manner.

CHAPTER 4

INSTRUMENTATION

The model crossflow tower was instrumented to obtain a description of its heat and mass transfer performance and to establish the validity of the computer program predictions. The parameters used to judge the tower's performance are the heat transfer rates (dry, wet and total) for given air and water flowrates and given air and water temperatures. To establish an energy balance between the air and water streams it is necessary to know the inlet and outlet temperatures for both fluids plus the flowrate of each. In addition, the air inlet and outlet humidity must be measured in order to calculate the evaporative heat transfer.

4.1 Temperature

Instrumentation of the counterflow tower is discussed in detail by Giebler [2]. This reference also gives the details of the calibration of the thermocouples used for monitoring temperature in the counterflow tower. The copper-constantan thermocouples used for that experiment were shown to have an approximate repeatability of .1°F (.06°C). These same thermocouples were used for temperature measurement in the crossflow tower.

To measure the air temperature rise across the packing section grids of 15 thermocouples each (5 equally spaced rows of 3 thermocouples each) were constructed in the inlet and outlet headers.

Readings from each grid of thermocouples were averaged to determine the average air inlet and outlet temperatures. Figure 8 shows the details of the water thermocouple instrumentation. To measure inlet water temperature, nine thermocouples were placed on the bottom of the water distribution box (A). Outlet water temperature was measured at 3 locations in the tower. First, water temperature was measured in the troughs at the bottom of one plate (B). Due to the large number of troughs on each plate, only 3 troughs were instrumented when testing the V-trough plates. All 7 troughs of one crossflow plate were instrumented. As a check of the water outlet temperature measured in the troughs, the collection pan (C) and trough (D) were also equipped with 3 thermocouples each. A switch box was used to connect the desired thermocouple to a digital voltmeter and reference ice bath.

Initial runs on the experimental apparatus showed a large variation in dry bulb temperature from top to bottom of the air inlet duct. Due to thermal stratification the air temperature at the top of the inlet was at times several degrees greater than the bottom air temperature. Proper placement of fans around the area in front of the air inlet eliminated this effect and produced a uniform air inlet temperature.

4.2 Humidity

Dewpoint at the air inlet and outlet was measured with an optical dewpoint hydrometer. Given the dewpoint, the actual water content of the air can be determined from tables. Because the laboratory

(intake) air was well mixed, no variation in dewpoint was observed across the inlet duct. Thus, measurement of ambient dewpoint defined the inlet air dewpoint. It would be expected that there might be some variation in humidity across the outlet duct. To avoid having to scan the outlet duct to determine the average outlet humidity, dewpoint was measured downstream of the fan. After traversing 14 feet (4.27 m) of duct and through the fan the air was considered well mixed. Discrepancies between dewpoint measured at this point and actual dewpoint at the packing section outlet could arise in two ways: leakage of ambient air into the duct or condensation of water on the inside of the duct walls. All joints in the ducting were taped to prevent the infiltration of ambient air. To avoid condensation inside the duct, the outlet dewpoint at any time during an experiment cannot be allowed to rise above the temperature of the duct walls. This condition never occurred during any of the experiments described here.

4.3 Water and Air Flowrate

Water flowrate was monitored by rotometer. For low flowrates, a rotometer with a maximum flowrate of 6.28 gpm (23.77 ℓ/min.) was used. For larger flowrates a 20.00 gpm (75.70 ℓ/min.) rotometer was available.

As mentioned in Section 2.4 a long section of duct downstream of the packing section was provided to allow air flow measurements. It was decided to permanently install a pitot tube in the center of the duct 10 ft. (3.05 m) downstream of the packing section exit. Measurements were then taken to relate the velocity measured at the duct centerline to

the average duct velocity. A relationship between the centerline and average velocity would then allow the average air mass flowrate to be calculated by measuring the centerline velocity. Air velocity scans across the duct diameter showed a fairly flat velocity profile. The velocity is nearly constant across the central portion of the duct. Only within about an inch (2.54 cm) does the velocity begin to decrease. Appendix B gives the airflow scan data and presents a polynomial curve fit $V(r)$ to the data. The pitot tube manufacturer lists a $\pm 2\%$ accuracy for airflow measurements under these conditions. Integration of this curve is performed to determine the average air velocity:

$$\bar{V} = \frac{\int_0^{r_o} V(r)(2\pi r dr)}{\pi r_o^2}$$

where r_o is the duct radius. The average air velocity is found to be $90 \pm 2\%$ of the centerline velocity measured by the fixed pitot tube.

CHAPTER 5

EXPERIMENTAL RESULTS AND COMPUTER PREDICTIONS

This chapter presents the experimental data taken from the crossflow experimental model tower and the corresponding predictions of the computer program. A general outline of the operation of the computer program is given first. There follows an explanation of the method used to reduce the experimental data. Next, the data is presented and discussed in two groups. The first group consists of experimental runs and computer predictions for the V-trough plates. The second group is data taken from the plates specifically designed for the crossflow configuration.

5.1 Computer Model

A listing of the crossflow computer model is given in Volume I. Essentially, the crossflow packing is modeled by the program as a grid of series exchangers, each of which has a small enough property change to be approximated by a counterflow heat exchanger. Along the top, the inlet water temperature is known. Along one side the inlet air temperature is known. The program starts in the upper corner of the grid where both air and water inlet conditions are known. Using heat and mass transfer relationships given in Reference [2], the outlet conditions for this section are calculated and the results used as inlet conditions for the grid sections below and directly to the side. By moving downward, one column at a time, using previously calculated outlet conditions for the adjoining grid squares, it is possible to calculate the performance of the entire packing section [3].

5.2 Analysis of Experiment

Overall enthalpy changes can be calculated using the instrumentation described in Chapter 4. The average intake and outlet temperatures are known for both the water and air streams. Air and water mass flowrates are known as are the average inlet and outlet water vapor content of the air. This data are sufficient to allow calculation of the enthalpy change for each fluid stream. Treating the packing section as a black box with no other energy streams, an energy balance can be established between the two streams. The water enthalpy loss multiplied by the water mass flowrate should equal the air enthalpy gain times the air mass flowrate.

The enthalpy change for the air was evaluated from tabulated values of dry air and water vapor enthalpies. For the air stream:

$$\Delta H_a = \dot{m}_a\{[h_{dry} + (h_{wv}\, w)]_{out} - [h_{dry} + (h_{wv}\, w)]_{in}\} \qquad (5\text{-}1)$$

where h_{dry} is the enthalpy of the dry air h_{wv} is the enthalpy of the water vapor and w is the specific humidity, all evaluated at inlet or outlet conditions. For the water stream:

$$\Delta H_\ell = \dot{m}_\ell\, c_\ell(T_{\ell out} - T_{\ell in}) + \Delta\dot{m}\, c_\ell(T_{\ell in} - T_o) \qquad (5\text{-}2)$$

Here the second term represents the enthalpy loss of the water stream due to evaporation. In practice c_ℓ was taken as 1 BTU/lbm-°F

(1 kcal/kf-°C) and $\Delta\dot{m}_\ell$ was calculated from the change in air specific humidity times the air mass flowrate:

$$\Delta\dot{m}_\ell = \dot{m}_a(w_{out} - w_{in}) \tag{5-3}$$

The evaporative heat transfer was computed by:

$$Q_{evap} = \Delta\dot{m}_\ell(h_{fg}^{T_{\ell in}} - C_v(T_{\ell in} - T_{\ell out}) \tag{5-4}$$

where c_v, the heat capacity of the water vapor, was taken to be .4458 BTU/lbm-°F (.4458 kcal/kgm-°C) and $H_{fg}^{T_{\ell in}}$ was taken from tabulated values.

The energy balance error was calculated from the equation:

$$\text{ERROR} = \frac{\Delta H_a - \Delta H_\ell}{\frac{1}{2}(\Delta H_a + \Delta H_\ell)} \tag{5-5}$$

A sample data reduction is presented in Appendix A. Given inlet conditions, the values of Q_{evap} and Q_{total} for the exhaust conditions were calculated by the computer model program. The following two sections present and discuss the data for the V-trough and crossflow packing sections.

5.3 V-Trough Crossflow Packing Section Performance

A summary of the experimental data and corresponding computer predictions for eight (8) test runs performed on the V-trough packing

plates are presented in Table 1. Table F-1 in Appendix F gives a more detailed account of the experimental data for each run. The tests were performed over a range of water flowrates and inlet temperatures. Inlet air humidity also varied but there was no significant change in air flowrate or air inlet temperature.

The experimental error, as defined previously, is an indicator of the accuracy of the experiment. Analysis of this particular experiment showed a maximum possible error in the total heat transferred of 15% [2] based on individual instrument repeatability. It can be seen that this limit was exceeded on several runs listed in Table 1, with the highest error being 20% for Run #6.

Experimentally, a good deal of difficulty was encountered in attempting to accurately measure the outlet water temperature. Of the three locations used to measure outlet water temperature listed in the instrumentation chapter, none proved to be consistent. The water temperature measured at the bottom of the plates was frequently several degrees less than that measured in the collection pan. This is a large change when compared to the total water temperature change which was about 10 degrees. This magnitude of temperature drop indicates that significant evaporation was occurring in the collection area after the water had fallen off the plates.

A study of the airflow in the V-groove packing section provided some insight into this problem. As discussed earlier, if the V-troughs present too large a profile to the oncoming air, a large pressure drop can result. In fact, this occurs in the V-trough packing section. In

TABLE 1

H_{dry} = 6.77

H_{wet} = 15.80

	RUN #1		RUN #2		RUN #3		RUN #4	
	Data		Data		Data		Data	
Air Flow Rate Lbm/min	110.0		109.9		106.6		106.6	
Inlet Water Flow Rate Lbm/min	69.75		133.4		81.8		83.0	
Inlet Air Temperature °F	84.0		82.0		79.4		79.7	
Inlet Humidity Lbm/Lbm	0.01287		.006886		.008565		.00889	
Average Heat Transfer BTU/min	1159	1059	1423	1285	1166	1217	1024	1056
Evaporative Heat Transfer BTU/min	587.7	575.0	810	717	651	659	589	565
Percent Evaporative Heat Transfer	51	54	57	56	56	54	57	54

	RUN #5		RUN #6		RUN #7		RUN #8	
	Data		Data		Data		Data	
Air Flow Rate Lbm/min	106.6		111.0		111.0		99.4	
Inlet Water Flow Rate Lbm/min	80.9		83.0		81.3		68.8	
Inlet Humidity Lbm/Lbm	.00889		.005358		.00476		.005859	
Inlet Water Temperature °F	128.0		130.3		128.0		130.5	
Average Heat Transfer BTU/min	920	938	1062	1066	1037	1027	970	
Evaporative Heat Transfer BTU/min	512	500	633	552	610	530	604	
Percent Evaporative Heat Transfer	56	53	60	52	59	52	62	

an attempt to avoid this large pressure drop, the air was observed in smoke studies to travel in the manner shown in Figure 14. The clearances above and below the packing section provided a path of lower resistance for the airflow.

The observed airflow pattern described above had several detrimental effects. Most important, the airflow was largest in the water distribution and collection areas. These are the areas that are most susceptible to evaporation due to the large water surface areas located there. This makes it impossible to separate the heat and mass transfer characteristic of the packing section from those of the distribution and collection systems. Since the computer program models only the characteristics of the packing section, good agreement between experimental data and computer predictions cannot be expected.

Another important aspect of the observed air flow pattern is its affect on the air flow pattern in the outlet duct. A nonhomogeneous airflow in the outlet duct will lead to outlet air temperature measurement errors. This is due to the fact that all 15 outlet air thermocouple readings are averaged together as if each represented the temperature of one-fifteenth of the flow. In fact, with a larger air flow at the top and bottom of the outlet header the top and bottom air thermocouple readings should be weighted heavier than the center readings. Air flow surveys to determine such a factor for each thermocouple would most likely reduce the experimental error. However, this would do nothing to cure the basic problem of the distorted airflow. In the last three runs an attempt was made to introduce baffles and flowblocks

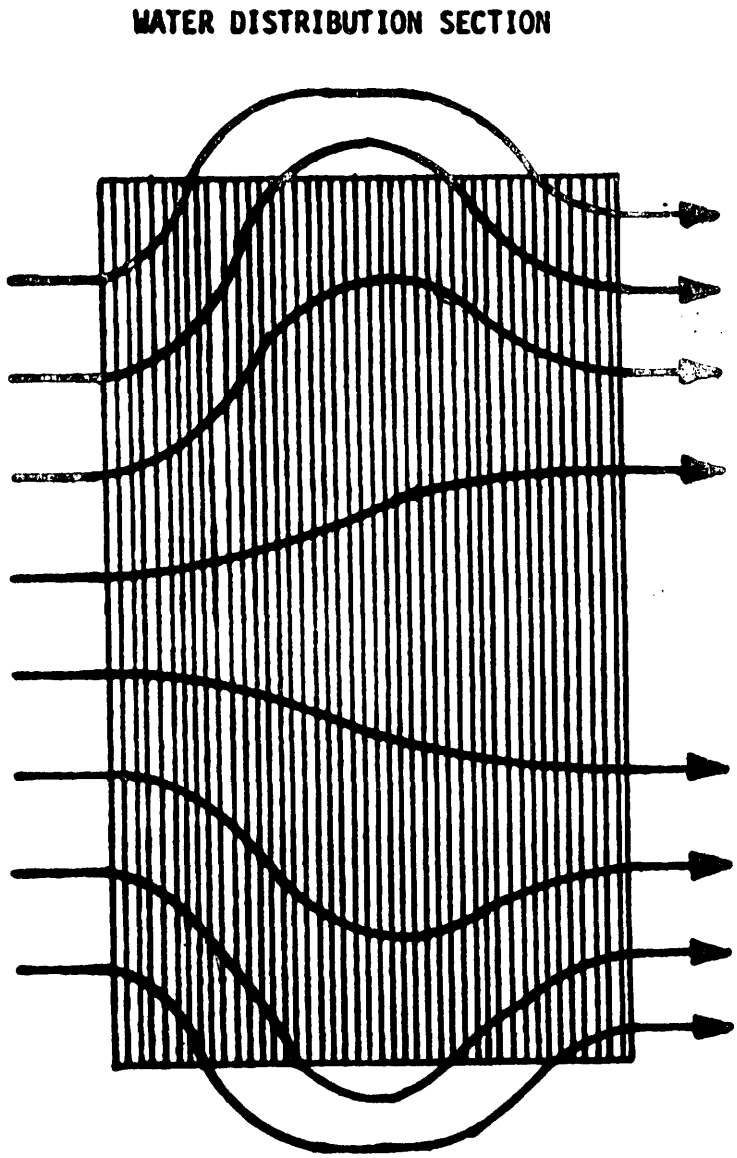

FIGURE 14. AIRFLOW OVER V-TROUGH PACKING PLATES

to redirect the airflow toward the center of the plates, but none had a significant effect on the airflow pattern.

Comparison of the computer predictions and the experimental data is difficult since the experimental data measures additional sources of evaporation. To compensate for this fact, the calculated mass transfer coefficient h_{evap} (originally calculated using the Dittus-Boelter relation and the Chilton-Colburn analogy between heat and mass transfer) was increased. However, it is likely that the total air-water interfacial area increased rather than h_{evap}. In general, the agreement between data and predictions obtained in this manner is good. The average heat transferred matches fairly well, especially in the later runs. In general, the predicted evaporative heat transfer is lower than that which is experimentally measured. Considering the water temperature measurement and airflow difficulties, agreement can be considered good. Computer predictions using calculated mass transfer coefficients suggested that the plates designed for crossflow, if they successfully reduced the air flowing over the distribution section, could be expected to lower the evaporative heat transfer to 30 or 40 percent of the total.

The V-trough experimental data serves as a useful guide to the type of trends that might be expected from the crossflow packing section. Total heat transfer increases as inlet water temperature or water flowrate increase. Also, evaporative heat transfer seems to be a strong function of inlet humidity, increasing with decreasing humidity. All of these observed trends are in fact reasonable to expect.

5.4 Crossflow Packing Plate Performance

The new crossflow plates were designed with the aim of reducing the pressure drop experienced by the air passing through the packing section. Also the baffling (described in the section dealing with the installation of these plates) provided much better isolation of the distribution and collection systems from the air streams. Thus, the experimental data and computer predictions presented here are a more valid test of the reliability of the computer program model. In addition, the onset of cold weather allowed a large variation in the inlet air temperature. Further modification of the experimental apparatus allowed tests to be performed at two different air flowrates.

A summary of the data and computer predictions is presented in Table 2, complete experimental data are given in Table F-2 in Appendix F. The experimental error for these 14 runs is much smaller than for the V-troughs. The water side energy balance is consistently low but the error is greater than 15% for run #10 only. The average error is 10%. With the exception of runs #4 and #5, there is very close agreement between the experimental evaporative heat transfer and the predicted value. It was observed during these two runs that the water did not always remain in the channels as it travelled down the plates. This has the effect of increasing the water surface area percentage above the design value (5%) that is used in the computer program. In this case it would be expected that the computer model would underpredict the evaporation. On this basis it can be assumed that the water flowrates

TABLE 2

HDP = 6.5
H = 8.0

	RUN #1		RUN #2		RUN #3		RUN #4		RUN #5	
Air Flow Rate Lbm/min	108.5		109.7		109.8		113.0		113.9	
Inlet Water Flow Rate Lbm/min	20.5		21.0		20.9		37.3		31.4	
Inlet Air Temperature F	79.1		79.3		78.9		70.8		76.8	
Inlet Air Humidity Lbm/Lbm x 10^3	3.183		3.163		2.850		3.505		3.849	
Inlet Water Temperature F	158.8		144.5		129.4		1.382		123.4	
Average Heat Transfer Rate BTU/min	627	650	498	516	364	388	590	544	390	369
Evaporative Heat Transfer BTU/min	276	262	206	199	145	144	255	186	174	129
Percent Evaporative Heat Transfer	44	40.3	41	39	39	37	43	34	45	35

	RUN #6		RUN #7		RUN #8		RUN #9		RUN #10	
Air Flow Rate Lbm/min	113.4		113.8		115.6		119.4		119.2	
Inlet Water Flow Rate Lbm/min	23.9		23.9		23.0		20.7		20.7	
Inlet Air Temperature F	57.9		56.4		55.7		35.6		30.7	
Inlet Air Humidity Lbm/Lbm x 10^3	4.894		4.844		.3807		.4180		.4117	
Inlet Water Temperature F	147.0		136.5		109.2		119.4		123.7	
Average Heat Transfer Rate BTU/min	627	645	549	556	318	342	489	508	580	591
Evaporative Heat Transfer BTU/min	213	199	170	157	87	78	102	98	127	117
Percent Evaporative Heat Transfer	34	31	31	28	28	23	21	19	22	20

TABLE 2 (CONT'D.)

	RUN #11		RUN #12		RUN #13		RUN #14	
Air Flow Rate Lbm/min	118.7		117.9		66.1		66.0	
Inlet Water Flow Rate Lbm/min	21.0		20.7		20.9		21.0	
Inlet Air Temperature F	29.1		28.4		81.0		80.9	
Inlet Air Humidity Lbm/Lbm x 10^3	.4117		.4244		4.648		4.648	
Inlet Water Temperature F	137.2		145.4		164.3		132.6	
Average Heat Transfer Rate BTU/min	667	675	752	748	528	536	305	303
Evaporative Heat Transfer BTU/min	149	145	191	172	233	222	129	113
Percent Evaporative Heat Transfer	22	21	25	23	44	41	42	37

for Runs 4 and 5 (which represent the highest water flowrates in this group of tests) are outside the operating range of these plates. A comparison of the average total heat transfer rates indicates that only in three cases (Runs 3, 4 and 8) was the difference larger than 5%. The largest disagreement is only 8% (run #4).

Appendix E demonstrates the method suggested by Reference [4] for calculating the heat and mass transfer coefficients for the ribbed surfaces. Over the conditions of these experiments the only variation that would significantly affect these coefficients is the difference in air flowrate for the last two runs. Thus, one set of transfer coefficients is valid for the first 12 runs and a different (lower) set is valid for the last two.

The following paragraphs will discuss the effect of the main variables on the performance of the tower. These variables are the air and water inlet temperatures and flowrates and the air humidity. For similar flow conditions it can be seen that the percent evaporative heat transfer is greatly reduced by lowering the air inlet temperature (compare runs 1, 2 and 3 with 8, 9 and 10). Actually, the amount of evaporative heat transfer is nearly unchanged but the increased temperature difference between the plate and the air (dry bulb) increases the sensible heat transfer. Thus, the efficiency of the wet/dry tower will be improved on colder days.

The effect of changing the water or air flowrate is similar. For given inlet conditions, lowering either flowrate lowers the total heat

transferred. Also, lowering either fluid flowrate increases the temperature change of that fluid and decreases the change of the other fluid. This is most easily seen by comparing Runs 1 and 13 where the air flowrate is reduced significantly.

Because there was no way to control the inlet humidity, the effect of varying humidity was more difficult to study experimentally. Runs 9 through 12 have very low inlet humidities but these runs were also done at low inlet air temperature so the humidity effect is difficult to uncover. Difference in mass concentration is the driving force behind evaporation of water into the air. Since humidity is a measure of water mass concentration in the air, it is reasonable to expect that increasing the inlet humidity would decrease the evaporation occurring in the tower.

These fourteen runs show that the evaporative heat transfer for the crossflow packing plates is in the range of 20% to 40% depending on the ambient temperature. For the same heat rejection load this represents a decrease of approximately 20% compared to the nonoptimal V-trough crossflow plates and about 15% compared to the V-trough counterflow results given by [2] and [3]. The evaporative heat transfer decrease is 50% or greater when compared to an all wet tower.

CHAPTER 6

CONCLUSIONS

6.1 Conclusions - Crossflow Model Tests

The crossflow design was found to offer significant advantages over the previous counterflow configuration. The most significant advantage was the simplicity of the crossflow design due to the elimination of the water headering problem.

The new crossflow packing plate had a 15 to 20 percent decrease in the percentage of evaporative heat transfer compared to the crossflow V-groove plates. It was felt that most of this reduction in evaporation was due to a reduction in air flow over the water in the water distribution and collection areas. This reduction in airflow in these areas was accomplished by minimizing the profile of the new crossflow plates and thus reducing the air pressure drop across the packing section. Also, baffles helped to channel the air stream away from the water distribution and collection areas.

Tests on the new counterflow plates showed that about 25 to 30 percent of the total heat transferred was evaporative. This represents a decrease of approximately 20% when compared to the crossflow V-trough packing section and about 15% when compared to the counterflow V-trough packing section. In addition, the evaporative heat transfer decrease

was 50% or greater when compated to an all wet tower.

The experimental results for 14 runs on the crossflow plates were compared to predictions of a computer model of the packing section. The heat and mass transfer coefficients for the model were calculated using correlations for ribbed surfaces. The agreement between prediction and experimental results was very good. The difference between predicted and measured total heat transfer was within 5% for all but 3 runs and never more than 8%. This accuracy is significant because it opens the way for use of the computer model for simulation or optimization of proposed full size wet/dry cooling towers.

6.2 Project Conclusions

Two years of experimentation and analysis have proven the effectiveness of the wet-dry packing plate in reducing cooling tower evaporation. Computer studies have predicted a yearly water consumption rate of 35-40% or less of that of a completely wet cooling tower under the same operating conditions.

The crossflow air-water arrangement has demonstrated the most promise for future development, offering simplicity and effectiveness as well as design flexibility.

A computer model, verified by experimental data has been written and is available for future design studies.

The cost of a wet-dry cooling system has been roughly figured and is competetive with the costs of alternative reduced-evaporation cooling systems.

Packing plates with the surface heat transfer coefficient augmented by roughening ribs have been constructed and tested in the laboratory

providing very good agreement with the original correlations for this type of surface.

In final conclusion, tests and analysis of the advanced wet-dry cooling tower concept have shown it to be an effective, simplified and competetive method of rejecting waste heat to the atmosphere at a reduced rate of water evaporation.

6.3 Future Work

Several design problems remain to be investigated before the concept can be moved into final development. These are:

1) Water distribution and collection. The present model design would probably not be practical on a large scale. A simpler design using shower sprays and water channeling sections in the packing would be better.

2) Determination of commercial packing plate materials and dimensions. The computer analogy could be used here to simulate the various possibilities under varying local conditions.

3) Manufacture of the packing plates. The roughening ribs used in the model were glued on individually. It may be possible to stamp or roll these grooves in the packing plate while it is being fabricated. Another potential savings could be realized by making the plate spacers and stiffeners an integral part of each packing plate.

4) Corrosion of the plate surface. This problem was avoided experimentally by painting and anodizing the two sets of plates tested. This problem occurs frequently with other types of cooling towers presently in use and its solution is very likely available within the industry.

5) Patent rights should be vigorously pursued and industrial involvement investigated so as to provide this cooling alternative to the power industry as soon as it is feasible to do so.

REFERENCES

1. Curcio, John L., Design and Development of an Advanced Wet/Dry Cooling Concept, M.S. Thesis, Dept. of Mechanical Engineering, M.I.T., August 1975.

2. Giebler, Martin M., Analysis and Testing of An Advanced Wet-Dry Cooling Tower, M.S. Thesis, Dept. of Mechanical Engineering, M.I.T., February 1976.

3. Snyder, T., Bentley, J., Giebler, M. Glicksman, L.R., Rohsenow, W.M., Advanced Wet-Dry Cooling Tower Concept-Performance Prediction, Vol. 1, MIT-EL 77-002, January 1977

4. Han, Je-Chin, Convective Heat Transfer Augmentation in Channels Using Repeated Rib Roughness, Sc.D. Thesis, Dept. of Mechanical Engineering, M.I.T., September 1976.

5. Rohsenow, W.M. and Choi, H.Y., Heat, Mass and Momentum Transfer, Prentice-Hall, Inc., Englewood Cliffs, New Jersey, 1971.

APPENDIX A

SAMPLE DATA REDUCTION

This Appendix demonstrates in detail the method used to reduce the experimental data. The data from Test #9 of the new crossflow plates will be used as an example. The raw data from test #9 is give first. The calculations leading to the data listed in Table 2 follows.

Experimental Data

Average Temperature:	Air Inlet	55.7"F	Water Inlet	109.2°F
	Outlet	64.2°F	Outlet	96.3°F
Air Dewpoint:	Inlet	38.14°F	Outlet	41.8°F

Pitot tube pressure .160 in/H_2O

Water flow = 23.0 lbm/min.

Barometric Pressure = 29.73 inches mercury

Step 1. Figure measured air density and velocity using pitot tube pressure and manufacturer's data:

$$\rho_{air} = 1.325 \frac{P_{Bar}}{T(°R)}$$

$$= 1.325 \frac{29.73}{(460+65)} = .07503 \text{ lbm/ft}^3$$

$$V_{\ell} = (1096.2) \left(\frac{.160}{.07503}\right)^{1/2} = 1601 \text{ ft/min}$$

Using the results of Appendix B,

$$V_{average} = .90\ V_{\text{¢}} = 1441 \text{ ft/min}$$

To figure the air mass flowrate:

$$\dot{m} = \rho A V_{average}$$

$$= (.07503)(\pi (\frac{13}{2})^2 \frac{1}{144}) 1441 = 115.6 \text{ lbm/min}$$

Using the average air (dry bulb) temperatures we refer to psychometric charts to find the enthalpy of dry air,

$$h_{dry} = \frac{\text{Inlet}}{5.6929} \quad \frac{\text{Outlet}}{7.7353} \text{ Btu/lbm air}$$

These same tables give the specific humidity at the inlet and outlet dewpoints

$$w = .004844 \qquad .005592 \text{ lbm water/lbm air}$$

The enthalpy of the moisture in the air is the product of the specific humidity listed above and the enthalpy of water vapor at the dry bulb temperature:

$$h_{water\ vapor} = 1085.6 \qquad 1089.3 \text{ Btu/lbm water}$$

$$h_{moisture} = 5.2582 \qquad 6.0942 \text{ Btu/lbm air}$$

The total enthalpy of the air then is the summation of the enthalpy of the dry air and the enthalpy of the moisture,

$$h_{tot} = 10.9511 \quad 13.8294 \text{ Btu/lbm air}$$

The total enthalpy charge is,

$$\Delta h_{tot} = 2.8783 \quad \text{Btu/lbm air}$$

The total energy charge of the air is the product of the total enthalpy charge and the air mass flowrate,

$$\Delta H_{total(air)} = (115.6)(2.8783) = 333 \text{ Btu/min}$$

The total energy charge of the water stream has two components as listed in Eq. (5-2).

$$\Delta H_{total(water)} = \dot{m}_{water}(T_{in} - T_{out}) + (\Delta w\, \dot{m}_{air})(T_{in(water)} - T_{ref})$$

$$= (23.0)(12.9) + .08644(109.2\ 32.0) = 303 \text{ Btu/min}$$

Error is given by Eq. (5-5),

$$\text{Error} = \frac{\Delta H_{water} - \Delta H_{air}}{\frac{1}{2}(\Delta H_{water} + \Delta H_{air})} = \frac{29}{318} = 9\%$$

The evaporative heat transfer is calculated from Eq. (5-4),

$$Q_{evap} = (.08644)(1030.45)(1096.2 - 64.2) = 87.3 \text{ Btu/min}$$

$$Q_{total} = \frac{1}{2}(\Delta H_{water} + \Delta H_{air}) = 318 \text{ Btu/min}$$

$$\text{Percent evaporation} = \frac{Q_{evap}}{Q_{total}} = \frac{87}{318} = 27\%$$

APPENDIX B

AIRFLOW CALCULATIONS

This Appendix presents the results of tests to determine the airflow through the tower. The aim of the experiments was to determine the average air velocity in the outlet duct leading to the fan and to then relate this average air velocity to the measured centerline velocity. By correlating the average and centerline velocities, it would then be possible to determine the average air velocity (and hence, the air mass flowrate through the tower) by just measuring the centerline velocity with a fixed pitot tube. In this manner the lengthy process of making an air velocity scan in the duct for each run could be avoided.

The fixed pitot tube was placed in the duct, 12 feet downstream of the packing section outlet header.

Boundary layer calculations suggested that at this point, the flow would not yet be fully developed. Therefore, it was expected that a scan across the diameter of the duct would show a relatively flat velocity profile in the center portions of the duct. The averaged results of 6 scans are shown in Table B-1. The scans were taken across two mutually perpendicular diameters of the 14" diameter duct.

The results in Table B-1 indicate that at a radius of 3 in. or less the velocity is fairly constant. For radii between 4 in. and 7 in. a polynomial curve fit was performed using Gauss elimination. This curve fit is given in Eq. (B-1) where r is now in feet and $V(r)$ in ft/min.

$$V(r) = -22040 + 270500r - 1131000\, r^2 + 2052663\, r^3 - 1367253\, r^4 \qquad \text{(B-1)}$$

TABLE B-1

radius (in)		Air Velocity (ft/min)	
wall	7	0	
	6 5/8	1020	curve fit
	5	1587	
	4	1600	
	3	1615	
	2	1617	constant velocity $V = V_{\ell}$
	1	1620	
centerline	0	1615	

The air volume flowrate through the duct is the product of the air velocity and the corresponding flow area Eq. (B-2),where the velocity

$$Q = VA \tag{B-2}$$

is not constant the volume flowrate is the integral of the velocity (as a function) of area times the differential area Eq. (B-3)

$$Q = \int_A V(A)\, dA = \int_r V(r)\, 2\pi r dr \tag{B-3}$$

Employing Eq. (B-2) for the duct area inside the 3" radius and Eq. (B-3) outside yields Eq. (B-4), the air volume flowrate in the duct

$$Q = r^2 V \Big|_{r=0}^{r=3/12} + \int_{r=3/12}^{r=7/12} 2\pi r dr\, V(r) \tag{B-4}$$

Substituting the experimental data from Table B-1 into Eq. (B-4):

$$Q = 1552 \text{ ft}^3/\text{min}$$

Now, the average air velocity is just the air volume flowrate divided by the duct area

$$\bar{V} = \frac{Q}{A_{duct}} = \frac{1552}{\pi(7/12)^2} = 1452 \text{ ft/min}$$

Therefore the ratio of average duct velocity to centerline velocity is

$$\frac{\bar{V}}{V_{\text{℄}}} = \frac{1452}{1615} = .90$$

For any similar airflow in the duct, the air mass flowrate can now be determined from the measured centerline velocity using Eq. (B-4),

$$\dot{m}_{air} = \rho A \bar{V} = \rho A_{duct}(.90\ V_{\text{℄}}) \qquad \text{(B-5)}$$

APPENDIX C

FIN EFFICIENCY CALCULATIONS FOR NEW CROSSFLOW PLATES

As described in the text, it was desirable to maintain a similar fin efficiency between the V-trough plates and the new aluminum crossflow plates. The fin efficiency η for the steel V-trough plates is .80. Thus, the spacing of the troughs on the new crossflow plates must be chosen to maintain this value. The plate cross-section is shown in Figure 15(A). The dry plate surface area is modelled as an aluminum fin with base temperature equal to the water temperature in the trough as shown in Figure 15(B). The length (L) of the fin for .80 fin efficiency is equal to one-half of the desired trough spacing. From Reference [5]:

Fin efficiency equation

$$\eta = \frac{T_{avh}}{mL} = .80 \qquad \text{(C-1)}$$

L = fin length

$$m = \sqrt{2h/Kt} \qquad \text{(C-2)}$$

h = heat transfer coefficient = 5 Btu/hr ft^2 °F

K = thermal conductivity of aluminum = 90 Btu/hr ft°F

t = plate thickness = .025 in

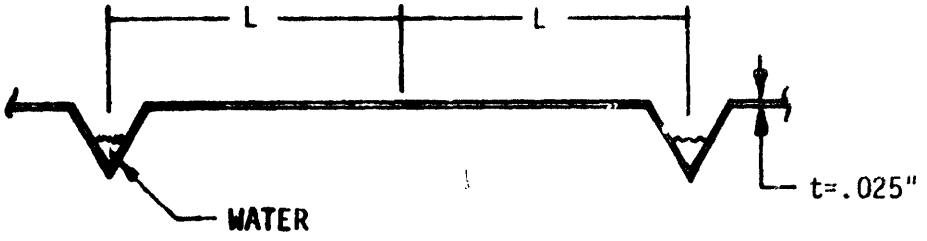

(A) PACKING PLATE CROSS-SECTION

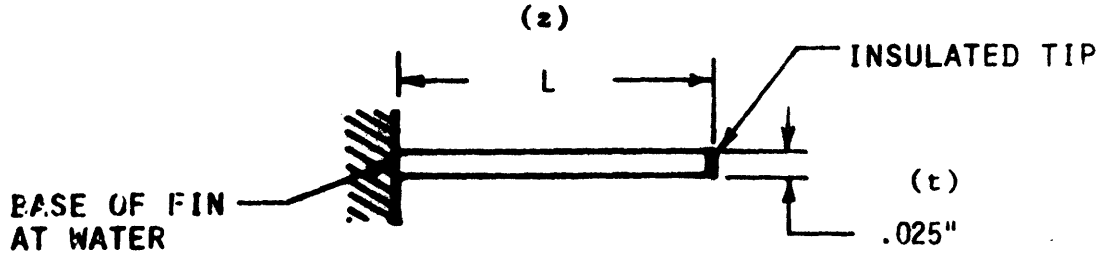

(B) APPROXIMATED FIN MODEL

REFERENCE (5)

$$\text{FIN EFFICIENCY, } \eta_f = \frac{\text{ACTUAL HEAT TRANSFER}}{\text{HEAT WHICH WOULD BE TRANSFERRED IF ENTIRE FIN AREA WERE AT THE BASE TEMPERATURE}}$$

$$\eta_f = 0.80$$

FIGURE 15. MODEL OF PACKING SECTION AS A FIN

Substituting these values into Eq. (C-2)

$$m = 6.35$$

Solving Eq. (C-1) for L we find

$$L = 1.5 \text{ inches}$$

Therefore the proper spacing of the channels for a plate efficiency of .80 is 2L or 3 inches. This was the method used to determine the plate spacing.

APPENDIX E

CALCULATION OF HEAT TRANSFER COEFFICIENTS FOR RIBBED SURFACES

This appendix demonstrates how the methods of Reference [4] were employed to determine the heat transfer coefficient h . The numbers used were typical of the experimental conditions for Runs 1 - 12 of the crossflow plates. Because optimal values were chosen for the height, spacing and angle of attack for the roughening ribs, the equations presented by Reference [4] are considerably simplified. The equations of interest here simplify to:

(4-1) [4]:

$$Re^+(e^+) = 4.9 \left(\frac{e^+}{35} \right) \qquad \text{(E-1)}$$

(2-13) [4]:

$$Re^+(e^+) = \sqrt{2/f} + 2.5 \, \ell n(2e/D_r) + 3.75 \qquad \text{(E-2)}$$

where e^+ is defined as:

$$e^+ = (e/D_h) \, Re \, \sqrt{f/2} \qquad \text{(E-3)}$$

(4-8) [2]:

$$(He^+) = 10.0 \, (e^+/35)^{.28} \qquad \text{(E-4)}$$

and

$$(Ee^+) = \left(\frac{f}{2\ S_{t-1}} \right) / \sqrt{f/2} + Re^+ \qquad \text{(E-5)}$$

Combining (E-1) and (E-2) yields:

$$(4\text{-}9) = \sqrt{2/f} + 2.5\ \ell n\left(\frac{2e}{D_h} \right) + 3.75 \qquad \text{(E-6)}$$

For the crossflow plates D_h = 3", e = .25" (e = rib height). Equation (E-6) can be solved to find

$$f = .06311$$

From Eq. (E-3) with Re = 15,300 between the plates:

$$e^+ = 227$$

Substituting this value into (E-4) gives,

$$He^+ = 16.9$$

The Stanton number can now be calculated from (E-5),

$$St = .010087$$

From the definition of the Stanton number,

$$St = nu/Re\ Pr \qquad \text{(E-7)}$$

and air properties we find the Nusselt number

$$Nu = 108$$

and hence the heat transfer coefficent ,

$$h = 6.9 \text{ Btu/hr ft}^2\text{°F}$$

used in the computer program for Runs 1 - 12 on the crossflow plates.

APPENDIX F DATA

TABLE F-1 H_{dry} = 6.77 H_{wet} = 15.80

	RUN #1		RUN #2		RUN #3		RUN #4	
	Data		Data		Data		Data	
Air Flow Rate Lbm/min	110.0		109.9		106.6		106.6	
Inlet Water Flow Rate Lbm/min	69.75		133.4		81.8		83.0	
Inlet Air Temperature °F	84.0		82.0		79.4		79.7	
Inlet Humidity Lbm/Lbm	0.01287		.006886		.008565		.0088662	
Inlet Water Temperature °F	135.9		138.1		139.0		132.6	
Outlet Air Temperature °F	97.7	99.8	102.8	100.5	99.0	98.3	97.2	96.5
Outlet Air Humidity Lbm/Lbm	0.01817	0.18060	.01418	.01339	.01467	.01472	.014083	.01391
Outlet Water Temperature °F	118.7	121.4	128.2	129.0	126.2	124.9	121.8	120.5
Air Temperature Change °F	13.7	15.8	20.0	18.5	19.6	18.9	17.5	16.8
Water Temperature Change °F	17.2	14.5	9.9	9.1	12.8	14.1	10.8	12.1
Air Humidity Change Lbm/Lbm	.00530		.00729		.00611		.00542	
Air Side Energy Balance BTU/min	1058		1440		1217		1094	
Water Side Energy Balance BTU/min	1259		1406		1116		954	
Average Heat Transfer BTU/min	1159	1059	1423	1285	1166	1217	1024	1056
Percent Error in Energy Balance	17		2		9		14	
Evaporative Heat Transfer BTU/min	587.7	575.0	810	717	651	659	589	565
Percent Evaporative Heat Transfer	51	54	57	56	56	54	57	54

TABLE F-1 (CONT'D.)

	RUN #5		RUN #6		RUN #7		RUN #8
Air Flow Rate Lbm/min	Data 106.6		Data 111.0		Data 111.0		Data 99.4
Inlet Water Flow Rate Lbm/min	80.9		83.0		81.3		68.8
Inlet Air Temperature °F	80.3		75.7		74.8		79.2
Inlet Humidity Lbm/Lbm	.00889		.005358		.00476		.005859
Outlet Air Temperature °F	96.4	95.4	93.2	92.9	92.3	91.6	94.4
Outlet Air Humidity Lbm/Lbm	.01360	.01352	.01104	.01028	.01026	.00950	.01191
Outlet Water Temperature °F	117.0	116.9	119.5	118.0	117.2	115.9	118.5
Air Temperature Change °F	16.1	15.1	17.5	17.2	17.5	16.8	15.2
Water Temperature Change °F	11.0	11.1	10.8	12.3	10.8	12.1	12.5
Air Humidity Change Lbm/Lbm	.00471		.00568		.00550		.00605
Air Side Energy Balance BTU/min	9011		1167		1138		1030
Water Side Energy Balance BTU/min	938		958		936		909
Average Heat Transfer BTU/min	920	938	1062	1066	1037	1027	970
Percent Error in Energy Balance	4		20		19		12
Evaporative Heat Transfer BTU/min	512	500	633	552	610	530	604
Percent Evaporative Heat Transfer	56	53	60	52	59	52	62

TABLE F-2 HDP = 6.5 H = 8.0

	RUN #1		RUN #2		RUN #3		RUN #4		RUN #5		RUN #6	
Air Flow Rate Lbm/min	108.4		109.7		109.8		113.0		113.9		113.4	
Inlet Water Flow Rate Lbm/min	20.5		21.0		20.9		37.3		31.4		23.9	
Inlet Air Temperature F	79.1		79.3		78.9		70.8		76.8		57.9	
Inlet Air Humidity Lbm/Lbm x 10^3	3.183		3.163		2.850		3.505		3.849		4.894	
Inlet Water Temperature F	158.8		144.5		129.4		138.2		123.4		147.0	
Outlet Air Temperature F	91.9	92.7	90.3	90.5	87.0	87.6	83.5	82.8	84.4	85.1	73.5	73.4
Outlet Air Humidity Lbm/Lbm x 10^3	5.801	5.633	5.071	4.983	4.173	4.151	5.784	5.036	5.420	4.963	6.677	6.613
Outlet Water Temperature F	131.0	128.3	123.0	120.7	113.2	111.4	124.3	124.1	111.9	112.0	123.0	120.8
Air Temperature F	12.8	13.6	11.0	11.2	8.1	8.7	12.7	12.0	7.6	8.3	15.6	15.5
Water Temperature Change F	27.8	30.5	21.5	23.7	15.2	18.0	13.9	14.1	11.4	11.4	24.0	26.2
Air Humidity Change Lbm/Lbm x 10^3	2.618		1.908		1.323		2.338		1.571		1.927	
Air Side of Energy Balance BTU/min	648		522	5	375		634		406		656	
Water Side of Energy Balance BTU/min	607		474		354		546		374		598	
Average Heat Transfer Rate BTU/min	627	650	498	516	364	388	590	544	390	369	627	645
Percent Error in Energy Balance	6%		9%		6%		15%		8%		9%	
Evaporative Heat Transfer BTU/min	276	262	206	199	145	144	255	186	174	129	213	199
Percent Evaporative Heat Transfer	94	40.3	41	39	39	37	43	34	45	35	34	31

TABLE F-2 (CONT'D.)

	RUN #7		RUN #8		RUN #9		RUN #10	
Air Flow Rate Lbm/min	113.8		115.6		119.4		119.2	
Inlet Water Flow Rate Lbm/min	23.9		23.0		20.7		20.7	
Inlet Air Temperature F	56.4		55.7		35.6		30.7	
Inlet Air Humidity Lbm/Lbm x 10^3	4.844		4.844		.3807		.4180	
Inlet Water Temperature F	136.5		109.2		119.4		123.7	
Outlet Air Temperature F	70.7	70.3	64.2	64.9	49.8	49.6	47.6	46.9
Outlet Air Humidity Lbm/Lbm x 10^3	6.354	6.223	5.592	5.506	1.2426	1.200	1.5090	1.400
Outlet Water Temperature F	115.6	113.8	96.3	94.6	97.6	95.2	102.5	99.5
Air Temperature Change F	14.3	13.9	8.5	9.2	10.2	14.0	14.7	16.2
Water Temperature Change F	20.9	22.7	12.9	14.7	21.8	24.2	25.2	28.2
Air Humidity Change Lbm/Lbm x 10^3	1.510		.7480		.8595		1.0910	
Air Side of Energy Balance BTU/min	581		333		519		625	
Water Side of Energy Balance BTU/min	517		303		460		534	
Average Heat Transfer Rate BTU/min	549	556	318	342	489	508	580	591
Percent Error in Energy Balance	12		9		12		16	
Evaporative Heat Transfer BTU/min	170	157	87	78	102	98	127	117
Percent Evaporative Heat Transfer	31	28	28	23	21	19	22	20

TABLE F-2 (CONT'D.)

	RUN #11		RUN #12		RUN #13		RUN #14	
Air Flow Rate Lbm/min	118.7		117.9		66.1		66.0	
Inlet Water Flow Rate Lbm/min	21.0		20.7		20.9		21.0	
Inlet Air Temperature F	29.1		28.4		81.0		80.9	
Inlet Air Humidity Lbm/Lbm x 10^3	.4117		.4244		4.648		4.648	
Inlet Water Temperature F	137.2		145.4		164.3		132.6	
Outlet Air Temperature F	48.1	47.2	49.5	48.1	99.6	98.9	92.3	92.1
Outlet Air Humidity Lbm/Lbm x 10^3	1.7012	1.637	2.098	1.906	8.283	8.066	6.428	6.344
Outlet Water Temperature F	108.2	105.6	113.5	110.4	142.3	139.9	118.9	118.6
Air Temperature Change °F	19.0	18.1	21.1	19.7	18.6	17.9	11.4	11.2
Water Temperature Change F	29.0	31.6	32.4	35.5	22.0	24.4	13.7	14.0
Air Humidity Change Lbm/Lbm x 10^3	1.2875		1.6736		3.635	3.418	1.780	1.696
Air Side of Energy Balance BTU/min	708		811		564		311	
Water Side of Energy Balance BTU/min	625		693		493		299	
Average Heat Transfer Rate BTU/min	667	675	752	748	528	536	305	303
Percent Error in Energy Balance	12		15		13		4	
Evaporative Heat Transfer BTU/min	149	145	191	172	233	222	129	113
Percent Evaporative Heat Transfer	22	21	25	23	44	41	42	37